Spatial Statistics 47 (2022) 100574

Contents lists available at ScienceDirect

Spatial Statistics

journal homepage: www.elsevier.com/locate/spasta

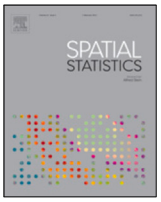

Blind source separation for non-stationary random fields

Christoph Muehlmann [a,*], François Bachoc [b], Klaus Nordhausen [c]

[a] Computational Statistics, Vienna University of Technology, Austria
[b] Institut de Mathématiques de Toulouse, Université Paul Sabatier, France
[c] Department of Mathematics and Statistics, University of Jyväskylä, Finland

ARTICLE INFO

Article history:
Received 30 June 2021
Received in revised form 7 December 2021
Accepted 13 December 2021
Available online 21 December 2021

Keywords:
Spatial statistics
Linear latent variable model

ABSTRACT

Regional data analysis is concerned with the analysis and modeling of measurements that are spatially separated by specifically accounting for typical features of such data. Namely, measurements in close proximity tend to be more similar than the ones further separated. This might hold also true for cross-dependencies when multivariate spatial data is considered. Often, scientists are interested in linear transformations of such data which are easy to interpret and might be used as dimension reduction. Recently, for that purpose spatial blind source separation (SBSS) was introduced which assumes that the observed data are formed by a linear mixture of uncorrelated, weakly stationary random fields. However, in practical applications, it is well-known that when the spatial domain increases in size the weak stationarity assumptions can be violated in the sense that the second order dependency is varying over the domain which leads to non-stationary analysis. In our work we extend the SBSS model to adjust for these stationarity violations, present three novel estimators and establish the identifiability and affine equivariance property of the unmixing matrix functionals defining these estimators. In an extensive simulation study, we investigate the performance of our estimators and also show their use in the analysis of a geochemical dataset which is derived from the GEMAS geochemical mapping project.

* Corresponding author.
E-mail address: christoph.muehlmann@tuwien.ac.at (C. Muehlmann).

https://doi.org/10.1016/j.spasta.2021.100574

1. Introduction

In spatial data analysis observations $x(\mathbf{s}_i)$, $i = 1, \ldots, n$ are collected in a domain $\mathcal{S} \subset \mathbb{R}^d$ where $\mathbf{s}_i \in \mathcal{S}$ specifies the location of the observation $x(\mathbf{s}_i)$. In most applications $d = 2$, which will be assumed in the following if not mentioned otherwise. It is meanwhile well-established that when analyzing spatial data the proximity of different sample locations has to be taken into account as observations located close to each other are expected to be more similar than observations further apart. The common way to consider this is via the covariance function

$$C_x(\mathbf{s}_i, \mathbf{s}_j) = \mathrm{E}\left((x(\mathbf{s}_i) - \mathrm{E}(x(\mathbf{s}_i)))(x(\mathbf{s}_j) - \mathrm{E}(x(\mathbf{s}_j)))\right). \tag{1}$$

To make working with spatial data more tractable one assumes that the spatial observations are realizations of a weakly stationary square-integrable random field which means one assumes that (i) $\mathrm{E}(x(\mathbf{s}_i)) = \mu$ for all $\mathbf{s}_i \in \mathcal{S}$ and that (ii) $C_x(\mathbf{s}_i, \mathbf{s}_j) = C_x(\mathbf{h})$, where $\mathbf{h} = \mathbf{s}_i - \mathbf{s}_j$ is the separation vector between the two considered sample locations. These assumptions state that the mean is constant over the domain and the covariance function is invariant under shifts. If additionally the covariance function does only depend on the distance $h = \|\mathbf{s}_i - \mathbf{s}_j\|$ then it is said to be isotropic. Usually, parametric covariance functions are specified and fitted to the data. One of the most popular parametric covariance functions is the isotropic stationary Matérn covariance function (Guttorp and Gneiting, 2006)

$$C(h; \sigma^2, \nu, \phi) = \frac{\sigma^2}{2^{\nu-1}\Gamma(\nu)} \left(\frac{h}{\phi}\right)^{\nu} K_\nu \left(\frac{h}{\phi}\right), \tag{2}$$

where K_ν is the modified Bessel function of second kind, Γ is the gamma function and $\sigma^2 > 0$, $\nu > 0$ and $\phi > 0$ are the variance, shape and range parameter respectively.

In many applications not only one variable is measured at each sample location but rather many, which yields multivariate spatial data where also cross-dependencies between the different variables have to be taken into account. Many suggestions and approaches for modeling the spatial cross-covariance functions for a p-variate random field $\mathbf{x}(\mathbf{s})$,

$$\mathbf{C}_\mathbf{x}(\mathbf{s}_i, \mathbf{s}_j) = E\left((\mathbf{x}(\mathbf{s}_i) - E(\mathbf{x}(\mathbf{s}_i)))(\mathbf{x}(\mathbf{s}_j) - E(\mathbf{x}(\mathbf{s}_j)))^\top\right) \tag{3}$$

are reviewed for example in Genton and Kleiber (2015) where it is also pointed out that it is not that easy to create flexible and valid spatial cross-covariance functions. One of the most popular approaches is the linear model of coregionalization (LMC) (Goulard and Voltz, 1992; Wackernagel, 2003), where the multivariate covariance function is formed by r summands of $p \times p$ positive semi-definite coregionalization matrices $\mathbf{T}_k$ multiplied by univariate, parametric spatial correlation functions $\rho_k(h)$. Formally, the LMC is stated as

$$\mathbf{C}(h) = \sum_{k=1}^{r} \mathbf{T}_k \rho_k(h). \tag{4}$$

Multivariate extensions of the Matérn covariance function are introduced by Gneiting et al. (2010) and Apanasovich et al. (2012). Specifically, Gneiting et al. (2010) formulate a model where the marginal and the cross-covariances are of the above Matérn covariance form. The marginal covariance functions yield

$$C_{ii}(h; \sigma_{ii}^2, \nu_{ii}, \phi_{ii}) = \sigma_{ii}^2 C(h; 1, \nu_{ii}, \phi_{ii}) \text{ for } i = 1, \ldots, p, \tag{5}$$

and the cross-covariances write as

$$C_{ij}(h; \rho_{ij}, \sigma_{ii}, \sigma_{jj}, \nu_{ij}, \phi_{ij}) = \rho_{ij}\sigma_{ii}\sigma_{jj} C(h; 1, \nu_{ij}, \phi_{ij}) \text{ for } i, j = 1, \ldots, p,\ i \neq j. \tag{6}$$

Conditions for the shape, range, variance and correlation parameters $\nu_{ij}, \phi_{ij}, \sigma_{ii}^2$ and ρ_{ij} for $i, j = 1, \ldots, p$ which result in a valid multivariate cross-covariance function can be formulated, however, these conditions are rather involved and therefore the interested reader is referred to Gneiting et al. (2010). Similar as in the univariate case, the two above families of cross-covariance functions, and many others, make the assumption of weak stationarity and isotropy.

As the domains in modern applications are however often huge it is meanwhile commonly accepted that the weak stationarity assumption is convenient but not realistic. Stationarity seems rather justifiable on a local scale but not globally. Thus, recent years saw an increased interest in developing spatial methods which do not assume weak stationarity where the focus was mainly on univariate approaches. For example Sampson (2010) reviews four different strategies to develop non-stationary covariance functions where the most popular approach seems to be based on spatial deformations. Anderes and Stein (2011) focus on extending the Matérn covariance for the non-stationary case by letting the shape, scale and variance parameters vary in the spatial domain. For the multivariate case Vu et al. (2021) point out that extensions of non-stationary cross-covariance functions are even more challenging to develop. Gelfand et al. (2004) extend the LMC to account for non-stationarity and Kleiber and Nychka (2012) extend the multivariate Matérn model, both by introducing spatially varying parameters. Vu et al. (2021) on the other side extend the spatial deformation approach to the multivariate setting and also review some other approaches. In any way all the discussed approaches start with the selection of one or more cross-covariance functions which are then fitted to the data.

Often, the analysis of multivariate spatial data is started with an exploratory step where the main goal is to find linear transformations of the data that are easy to interpret and show the main features. A natural first candidate of suitable methods would be the classical principal component analysis (PCA). However, PCA treats the data as an iid sample discarding the possible spatial dependence completely. Efforts of accounting for spatial dependence in the context of PCA have been made in the literature. The geographically weighted principal component analysis (Harris et al., 2015; Cartone and Postiglione, 2021) considers spatial dependence by carrying out the eigenvalue decomposition of locally weighted covariance matrices resulting in a set of different loadings for each sample location. A different direction is taken by Nordhausen et al. (2015) and Bachoc et al. (2020) where the methodology of blind source separation (BSS) (Comon and Jutten, 2010) is combined with (stationary) geostatistics (Bailey and Krzanowski, 2012) denoted as spatial blind source separation (SBSS). In SBSS it is assumed that the observable random field is formed by the so-called location scatter model

$$\mathbf{x}(\mathbf{s}) = \mathbf{A}\mathbf{z}(\mathbf{s}) + \mathbf{b}. \tag{7}$$

Here, $\mathbf{x}(\mathbf{s})$ and $\mathbf{z}(\mathbf{s})$ are the observed and latent random fields where the latter one consists of p uncorrelated/independent stationary entries. $\mathbf{A}$ and $\mathbf{b}$ are the invertible mixing matrix and a location vector. The aim of SBSS is to recover the latent field by simultaneous/joint diagonalization of so-called local covariance matrices. Joint diagonalization of suitable matrices is already considered in spatial data analysis by De Iaco et al. (2013) and Cappello et al. (2021) where the joint diagonalizer is restricted to be orthogonal which is not the case for SBSS. Recovering $\mathbf{z}(\mathbf{s})$ has great advantages as the interpretations of the resulting components follow the same scores-loadings principle as in PCA and the uncorrelatedness/independence property allows for further univariate modeling. The latter property is investigated in Muehlmann et al. (2021d) in the context of spatial prediction. In this publication it is pointed out that when applying SBSS prior spatial prediction the task of modeling the univariate data (cross-dependencies) can be discarded in favor of p univariate models. E.g.: The univariate predictions might be carried out with simple methods such as inverse distance weighting, various forms of Kriging, more sophisticated methods such as neural networks (Wang et al., 2019), general statistical/machine learning methods (Li and Heap, 2014; Jiang, 2019) or specifically for the non-stationary case designed methods such as the one given in Thakur et al. (2018). Note that the covariance structure of the above location-scatter model yields a special case of an LMC leading to rank-one coregionalization matrices and $r = p$, see Bachoc et al. (2020) for details. Hence, predictions of the latent field entries might be viewed as predicting the factors leading to a LMC which is considered by factorial Kriging, see Goovaerts (1992) or Wackernagel (2003, Chapter 27).

Our main contribution is to state a second order spatial non-stationary blind source separation model (the non-constant drift case is investigated in Muehlmann et al., 2021b) which is a reformulation of the already known non-stationary time series model in the first part of Section 2. Moreover, as SBSS is a relatively new field in the spatial statistics community we concisely present desired properties of general BSS unmixing matrix functionals in the second part of Section 2. Section 3

adapts the non-stationary time series estimators for the model outlined in Section 2 and studies the identifiability and affine equivariance properties of the underlying unmixing matrix functionals. The core of the work is formed by extensive simulation studies in Section 4 and the analysis of a geochemical dataset in Section 5 which are meant to persuade the spatial readership to account for the practical usefulness of the introduced methods. Lastly, we conclude the paper in Section 6 and hint ideas for further research. The appendix contains the proofs of the stated propositions and more simulation results.

2. A non-stationary spatial blind source separation model

For the remainder of the paper we assume that the random field $\mathbf{x}(\mathbf{s})$ at hand follows a spatial non-stationary (blind) source separation (SNSS) model which is defined as follows.

Definition 1 (*Spatial Non-Stationary Source Separation Model*)**.** A p-variate random field $\mathbf{x}(\mathbf{s})$ defined on a d-dimensional spatial domain $\mathcal{S} \subseteq \mathbb{R}^d$ follows a spatial non-stationary source separation model (SNSS) if it can be formulated as

$$\mathbf{x}(\mathbf{s}) = \mathbf{A}\mathbf{z}(\mathbf{s}) + \mathbf{b}, \tag{8}$$

where $\mathbf{A}$ is a deterministic invertible $p \times p$ mixing matrix, $\mathbf{b}$ is a p-variate deterministic location vector and $\mathbf{z}(\mathbf{s})$ is a p-variate latent random field which fulfills the following assumptions

(SNSS 1) $\mathrm{E}(\mathbf{z}(\mathbf{s})) = \mathbf{0}$ for all $\mathbf{s} \in \mathcal{S}$,
(SNSS 2) $\mathrm{Cov}(\mathbf{z}(\mathbf{s})) = \mathrm{E}\left(\mathbf{z}(\mathbf{s})\mathbf{z}(\mathbf{s})^\top\right) = \boldsymbol{\Sigma}_{\mathbf{s}}$ where $\boldsymbol{\Sigma}_{\mathbf{s}}$ is a positive definite diagonal matrix for all $\mathbf{s} \in \mathcal{S}$ and
(SNSS 3) $\mathrm{Cov}(\mathbf{z}(\mathbf{s}), \mathbf{z}(\mathbf{s}')) = \mathrm{E}(\mathbf{z}(\mathbf{s})\mathbf{z}(\mathbf{s}')^\top) = \boldsymbol{\Sigma}_{\mathbf{s}\mathbf{s}'}$, for all $\mathbf{s} \neq \mathbf{s}' \in \mathcal{S}$ where $\boldsymbol{\Sigma}_{\mathbf{s}\mathbf{s}'}$ is a diagonal matrix depending on $\mathbf{s}$ and $\mathbf{s}'$.

In practical considerations the random field $\mathbf{x}(\mathbf{s})$ of Definition 1 is observed on a set of n deterministic sample locations $\mathcal{C} = \{\mathbf{s}_1, \ldots, \mathbf{s}_n\} \subset \mathcal{S}$ which is a natural assumption for geostatistical applications. The domain $\mathcal{S}$ can be thought of as a continuous version of the sample locations $\mathcal{C}$ and can in principle be of any shape, but for convenience it is often a d-dimensional hyperrectangle, which so-to-speak covers $\mathcal{C}$.

Assumption (SNSS 1) states that the mean of each entry of the latent random field is a constant for the whole domain. In contrast, assumptions (SNSS 2) and (SNSS 3) allow the diagonal covariance as well as the diagonal spatial cross-covariance matrices to be dependent on the specific sample locations. In total, the observed random field is formed by uncorrelated latent random fields that are non-stationary in the sense that the second order dependencies are allowed to vary across the spatial domain. Often however the assumption of uncorrelated latent components is replaced by the stronger assumption of mutual independence. For general overviews of blind source separation (BSS) methods and their assumptions see for example Comon and Jutten (2010) and Nordhausen and Oja (2018). The SNSS model here can be seen as a spatial variant of the non-stationary time series model which is for example considered in Choi and Cichocki (2000a,b), Choi et al. (2001) and Nordhausen (2014).

If (SNSS 2) and (SNSS 3) are forced to be stationary, i.e, $\boldsymbol{\Sigma}_{\mathbf{s}}$ is constant and the diagonal matrix $\boldsymbol{\Sigma}_{\mathbf{s}\mathbf{s}'}$ carries stationary covariance functions on its diagonal elements, i.e. functions only of the difference vector $\mathbf{h}$ between $\mathbf{s}$ and $\mathbf{s}'$, then the model of Definition 1 corresponds to the (stationary) SBSS model discussed in detail in Nordhausen et al. (2015) and Bachoc et al. (2020).

The main goal of SNSS is to recover the true latent random field $\mathbf{z}(\mathbf{s})$ based on $\mathbf{x}(\mathbf{s})$ alone. Thus, an unmixing matrix functional $\mathbf{W} = \mathbf{W}(\mathbf{x}(\mathbf{s}))$ and a location functional $\mathbf{T} = \mathbf{T}(\mathbf{x}(\mathbf{s}))$ are required such that $\mathbf{z}(\mathbf{s}) = \mathbf{W}(\mathbf{x}(\mathbf{s}))\,(\mathbf{x}(\mathbf{s}) - \mathbf{T}(\mathbf{x}(\mathbf{s})))$. Note that assumptions (SNSS 1)-(SNSS 3) are not sufficient to make this a well-defined problem as the conditions do not fix the order, signs and scales of the latent components of $\mathbf{z}(\mathbf{s})$. That is, let $\mathbf{J} = \mathbf{PSD}$ where $\mathbf{P}$ denotes a permutation matrix, $\mathbf{S}$ a sign-change matrix and $\mathbf{D}$ a diagonal matrix with positive diagonal values. Then, the pairs $(\mathbf{A}, \mathbf{z}(\mathbf{s}))$ and $(\mathbf{A}\mathbf{J}^{-1}, \mathbf{J}\mathbf{z}(\mathbf{s}))$ both lead to the same $\mathbf{x}(\mathbf{s})$ and fulfill all requirements of Definition 1, hence, they are not distinguishable. This leads to the fact that recovering $\mathbf{z}(\mathbf{s})$ is only possible up to order, signs and

scale which is an ambiguity present in all BSS models and not considered a problem. For a detailed discussion about identifiability and general ambiguities in BSS models see for example Bachoc et al. (2020), Tong et al. (1991) and Eriksson and Koivunen (2004).

Another requirement of unmixing matrix functionals is the affine equivariance property (Miettinen et al., 2015) which states that the same latent random field is recovered (up to order and sign) independent of the exact way of mixing. Let $\mathbf{x}(\mathbf{s})$ be a random field and $\mathbf{x}^*(\mathbf{s}) = \mathbf{B}\mathbf{x}(\mathbf{s}) + \mathbf{a}$ its affine transformed version, where $\mathbf{B}$ is any invertible $p \times p$ matrix and $\mathbf{a}$ is any p-dimensional vector. For an affine equivariant unmixing matrix functional it holds that $\mathbf{W}(\mathbf{B}\mathbf{x}(\mathbf{s})+\mathbf{a}) = \mathbf{W}(\mathbf{x}(\mathbf{s}))\mathbf{B}^{-1} = \mathbf{A}^{-1}\mathbf{B}^{-1}$ up to order and sign of the row vectors. Multivariate statistical tools fulfilling this property belong to the more general invariant coordinate system (ICS) framework (Ilmonen et al., 2012).

The following definition formally states identifiability and the affine equivariance property of unmixing matrix functionals discussed before.

Definition 2 (*Unmixing Matrix Functional*)**.** For a random field $\mathbf{x}(\mathbf{s})$ following the SNSS model (Definition 1) a $p \times p$ matrix-valued functional $\mathbf{W}(\mathbf{x}(\mathbf{s}))$ is an unmixing matrix functional if it satisfies:

(Identifiability) $\mathbf{W}(\mathbf{x}(\mathbf{s}))\mathbf{A} = \mathbf{PSD}$ for some permutation matrix $\mathbf{P}$, sign change matrix $\mathbf{S}$ and diagonal matrix with strictly positive diagonal elements $\mathbf{D}$.

(Affine equivariance) $\mathbf{W}(\mathbf{B}\mathbf{x}(\mathbf{s}) + \mathbf{a}) = \mathbf{PSW}(\mathbf{x}(\mathbf{s}))\mathbf{B}^{-1}$ where $\mathbf{B}$ is an invertible $p \times p$ matrix, $\mathbf{a}$ is a p-dimensional vector, $\mathbf{P}$ is some permutation matrix and $\mathbf{S}$ is some sign change matrix.

In the subsequent section we introduce three unmixing matrix functionals that solve the above stated SNSS problem and investigate their identifiability and affine equivariance properties.

3. Three SNSS methods

The goal of this section is to introduce three different unmixing matrix functionals $\mathbf{W}(\mathbf{x}(\mathbf{s}))$ that can be used in conjunction with any location functional $\mathbf{T}(\mathbf{x}(\mathbf{s}))$ to recover the latent random field $\mathbf{z}(\mathbf{s})$ by $\mathbf{W}(\mathbf{x}(\mathbf{s}))\,(\mathbf{x}(\mathbf{s}) - \mathbf{T}(\mathbf{x}(\mathbf{s})))$. For $\mathbf{T}(\mathbf{x}(\mathbf{s}))$ we simply use the expectation and in the following focus our discussion solely on $\mathbf{W}(\mathbf{x}(\mathbf{s}))$. The key quantities for all three following unmixing matrix functionals are so-called local covariance matrices which are defined as

$$\mathbf{M}_{\mathcal{S},f}(\mathbf{x}(\mathbf{s})) = \frac{1}{|\mathcal{S} \cap \mathcal{C}|} \sum_{\mathbf{s}_i,\mathbf{s}_j \in \mathcal{S}\cap\mathcal{C}} f(\mathbf{s}_i - \mathbf{s}_j)\mathrm{E}\Big[[\mathbf{x}(\mathbf{s}_i) - \mathrm{E}(\mathbf{x}(\mathbf{s}_i))][\mathbf{x}(\mathbf{s}_j) - \mathbf{E}(\mathbf{x}(\mathbf{s}_j))]^\top\Big]. \tag{9}$$

Local covariance matrices were introduced in Nordhausen et al. (2015) and refined in Bachoc et al. (2020) and Muehlmann et al. (2020) in the context of SBSS for the second order stationary case. Note that in Eq. (9) we allow the considered spatial domain $\mathcal{S}$ not to contain $\mathcal{C}$ which is slightly different in comparison with the original definition, this will be useful when considering subdomains below. The matrices $\mathbf{M}_{\mathcal{S},f}(\mathbf{x}(\mathbf{s}))$ compute a weighted average of the spatial covariances of all available pairs of coordinates $\mathcal{S}\cap\mathcal{C}$, where the weights are determined by the so-called spatial kernel function $f : \mathbb{R}^d \to \mathbb{R}$. Three options are introduced in Bachoc et al. (2020) as follows.

- **Ball kernel:** $f_b(\mathbf{s}; r) = I(\|\mathbf{s}\| \leq r)$ where $r \geq 0$.
- **Ring kernel:** $f_r(\mathbf{s}; r_1, r_2) = I(r_1 < \|\mathbf{s}\| \leq r_2)$ where $r_1, r_2 \geq 0$ and $r_1 < r_2$.
- **Gauss kernel:** $f_g(\mathbf{s}; r) = \exp(-0.5(\Phi^{-1}(0.95)\|\mathbf{s}\|/r)^2)$ where $r > 0$ and $\Phi^{-1}(0.95)$ is the 95% quantile of the standard Normal distribution.

Here $I(\cdot)$ denotes the indicator function. All three kernel functions above assume isotropic random fields as they only operate on the norm of $\mathbf{s}$. It is possible to define spatial kernel functions differently and account for possible anisotropies present in the random fields, this is however beyond the scope of this paper.

For the special case of a ball kernel with parameter $r = 0$, denoted as f_0, local covariance matrices reduce to the average covariance in $\mathcal{S}$ where no spatial dependence is utilized. Formally

$$\mathbf{M}_{\mathcal{S},f_0}(\mathbf{x}(\mathbf{s})) = \frac{1}{|\mathcal{S} \cap \mathcal{C}|} \sum_{\mathbf{s}\in\mathcal{S}\cap\mathcal{C}} \mathrm{E}\Big[[\mathbf{x}(\mathbf{s}) - \mathrm{E}(\mathbf{x}(\mathbf{s}))][\mathbf{x}(\mathbf{s}) - \mathbf{E}(\mathbf{x}(\mathbf{s}))]^\top\Big]. \tag{10}$$

Considering a finite sample, the estimation of the subsequently introduced mixing matrix functionals is carried out by replacing the population quantities from Eq. (9) by their sample counterparts. Specifically, the corresponding sample version of Eq. (9) is given by

$$\hat{\mathbf{M}}_{\mathcal{S},f}(\mathbf{x}(\mathbf{s})) = \frac{1}{|\mathcal{S}\cap\mathcal{C}|}\sum_{\mathbf{s}_i,\mathbf{s}_j\in\mathcal{S}\cap\mathcal{C}} f(\mathbf{s}_i-\mathbf{s}_j)(\mathbf{x}(\mathbf{s}_i)-\bar{\mathbf{x}})(\mathbf{x}(\mathbf{s}_j)-\bar{\mathbf{x}})^\top, \tag{11}$$

where $\bar{\mathbf{x}} = n^{-1}\sum_{i=1}^n \mathbf{x}(\mathbf{s}_i)$, which also defines the sample version of $\mathbf{M}_{\mathcal{S},f_0}(\mathbf{x}(\mathbf{s}))$. Additionally, we estimate the location functional $\mathbf{T}(\mathbf{x}(\mathbf{s}))$ always by $\bar{\mathbf{x}}$.

For a random field $\mathbf{x}(\mathbf{s})$ following the SNSS model (Definition 1) we observe that $\mathbf{M}_{\mathcal{S},f_0}(\mathbf{z}(\mathbf{s}))$ as well as $\mathbf{M}_{\mathcal{S},f}(\mathbf{z}(\mathbf{s}))$ yield diagonal matrices for all formerly discussed kernel function options which motivates the following three estimators.

3.1. Simultaneous diagonalization of two average covariance matrices

The first unmixing matrix functional is based on the simultaneous diagonalization (sd) of two average covariance matrices which is formalized in the following definition.

Definition 3 (*SNSS.sd Functional*)**.** Consider a random field $\mathbf{x}(\mathbf{s})$ following the SNSS model (Definition 1) and a partition of the spatial domain $\mathcal{S}$ into $\mathcal{S}_1, \mathcal{S}_2$ where $\mathcal{S}_1\cap\mathcal{S}_2 = \emptyset$. The SNSS.sd functional $\mathbf{W} = \mathbf{W}(\mathbf{x}(\mathbf{s}))$ is defined as the simultaneous diagonalizer satisfying

$$\mathbf{W}\mathbf{M}_{\mathcal{S}_1,f_0}(\mathbf{x}(\mathbf{s}))\mathbf{W}^\top = \mathbf{I}_p \quad \text{and} \quad \mathbf{W}\mathbf{M}_{\mathcal{S}_2,f_0}(\mathbf{x}(\mathbf{s}))\mathbf{W}^\top = \mathbf{D}_{\mathcal{S}_1\mathcal{S}_2}, \tag{12}$$

where $\mathbf{D}_{\mathcal{S}_1\mathcal{S}_2}$ is a diagonal matrix with decreasingly ordered diagonal elements.

Given a sample, an unmixing matrix $\mathbf{W}$ can be found by solving the generalized eigenvalue–eigenvector problem, which always yields exact diagonalization of the former two matrices. Furthermore, the decreasing ordering of the diagonal elements of $\mathbf{D}_{\mathcal{S}_1\mathcal{S}_2}$ comes without loss of generality as the order of the latent random field can be anyhow only recovered up to permutations. The following proposition gives a necessary condition for the identifiability of the above unmixing matrix functional as well as the desired affine equivariance property.

Proposition 1. *The SNSS.sd functional seen in Definition 3 is*

(1) *identifiable as seen in Definition 2 if and only if elements of the diagonal matrix* $\mathbf{M}^{-1}_{\mathcal{S}_1,f_0}(\mathbf{z}(\mathbf{s}))\mathbf{M}_{\mathcal{S}_2,f_0}(\mathbf{z}(\mathbf{s}))$ *are pairwise distinct,*
(2) *affine equivariant as seen in Definition 2.*

Following Nordhausen (2014, Result 1), identifiability is ensured if there exist at least two sample locations $\mathbf{s}_1, \mathbf{s}_2 \in \mathcal{C} \subset \mathcal{S}$ for which the diagonal elements of the diagonal matrix $\boldsymbol{\Sigma}^{-1}_{\mathbf{s}_1}\boldsymbol{\Sigma}_{\mathbf{s}_2}$ are pairwise distinct (where $\boldsymbol{\Sigma}_{\mathbf{s}_1}$ and $\boldsymbol{\Sigma}_{\mathbf{s}_2}$ refer to the covariance matrices of the latent field at the corresponding sample locations $\mathbf{s}_1, \mathbf{s}_2$, see also Definition 1). If the former holds then it is possible to find two disjoint sub-domains $\mathcal{S}_1, \mathcal{S}_2$ of $\mathcal{S}$ in such a way that all elements of the diagonal matrix $\mathbf{M}^{-1}_{\mathcal{S}_1,f_0}(\mathbf{z}(\mathbf{s}))\mathbf{M}_{\mathcal{S}_2,f_0}(\mathbf{z}(\mathbf{s}))$ are pairwise distinct. Note that Nordhausen (2014, Result 1) is formulated for the times series non-stationary blind source separation model, the above outline is the natural extension of this statement to the spatial non-stationary case. However, in practical considerations the desired partition is unknown, therefore the a-priori choice of the partition of the domain is not trivial and greatly affects the performance of the method. This issue is addressed in the following extension of the former unmixing matrix functional.

3.2. Joint diagonalization of more than two average covariance matrices

In contrast to the former method the spatial domain is divided into more than two subdomains and the corresponding average covariance matrices are jointly diagonalized (jd) as follows.

Definition 4 (*SNSS.jd Functional*)**.** Consider a random field $\mathbf{x}(\mathbf{s})$ following the SNSS model (Definition 1). Standardize $\mathbf{x}(\mathbf{s})$ by $\mathbf{x}^{st}(\mathbf{s}) = \mathbf{M}^{-1/2}_{\mathcal{S},f_0}(\mathbf{x}(\mathbf{s}))(\mathbf{x}(\mathbf{s}) - \mathbf{b})$ and partition the spatial domain $\mathcal{S}$ into $\mathcal{S}_1, \ldots, \mathcal{S}_K$ where $\mathcal{S}_m \cap \mathcal{S}_n = \emptyset$ for $m, n = 1, \ldots, K$ and $m \neq n$. Let $\mathbf{U}$ be the orthogonal $p \times p$ joint diagonalizer of the matrices $\mathbf{M}_{\mathcal{S}_k,f_0}(\mathbf{x}^{st}(\mathbf{s}))$ for $k = 1, \ldots, K$, which maximizes

$$\sum_{k=1}^{K} \|\mathrm{diag}(\mathbf{U}\mathbf{M}_{\mathcal{S}_k,f_0}(\mathbf{x}^{st}(\mathbf{s}))\mathbf{U}^\top)\|_F^2. \tag{13}$$

Then, the SNSS.jd functional equals $\mathbf{W}(\mathbf{x}(\mathbf{s})) = \mathbf{U}\mathbf{M}^{-1/2}_{\mathcal{S},f_0}(\mathbf{x}(\mathbf{s}))$.

In the above definition $\mathrm{diag}(\cdot)$ is a diagonal matrix with the diagonal elements equaling the ones of the matrix-valued argument, and $\|\cdot\|_F$ denotes the Frobenius norm. $\mathbf{U}$ is denoted an orthogonal joint diagonalizer of the matrices $\mathbf{M}_{\mathcal{S}_k,f_0}(\mathbf{x}^{st}(\mathbf{s}))$ for $k = 1, \ldots, K$ as maximizing the diagonal elements is equal to minimize the off-diagonal elements by the orthogonal invariance of the Frobenius norm. Note that for a finite sample, usually the sample versions of the matrices $\mathbf{M}_{\mathcal{S}_k,f_0}(\mathbf{x}^{st}(\mathbf{s}))$ for $k = 1, \ldots, K$ given by Eq. (11) do not commute, hence, exact joint diagonalization is impossible. Therefore, algorithms that find an approximate joint diagonalizer are needed. We choose one such algorithm that relies on Givens rotations (Cardoso and Souloumiac, 1996), but many others are available, see for example Illner et al. (2015).

The next proposition is concerned with identifiability as well as affine equivariance.

Proposition 2. *The SNSS.jd functional seen in Definition 4 is*

(1) *identifiable iff for all pairs $i, j = 1, \ldots, p$ and $i \neq j$ there exists a $k \in \{1, \ldots, K\}$ such that $(\mathbf{M}^{-1}_{\mathcal{S},f_0}(\mathbf{z}(\mathbf{s}))\mathbf{M}_{\mathcal{S}_k,f_0}(\mathbf{z}(\mathbf{s})))_{ii} \neq (\mathbf{M}^{-1}_{\mathcal{S},f_0}(\mathbf{z}(\mathbf{s}))\mathbf{M}_{\mathcal{S}_k,f_0}(\mathbf{z}(\mathbf{s})))_{jj}$,*

(2) *affine equivariant as seen in Definition 2.*

The condition for identifiability given in Proposition 2 is more general than the one in Proposition 1 as a finer partition of the domain is allowed. Therefore, the exact partition of the domain for the SNSS.jd method should have less influence on the performance as long as enough sub-domains are considered. In practical applications it might be useful to overlay the spatial domain by a grid which is formed by equally sized squared shaped blocks. These blocks are meant to define the subdivision of $\mathcal{S}$. This procedure is investigated in more detail in the simulation study in Section 4. The advantage of less sensitivity on the exact domain sub-partition of the SNSS.jd methods comes at the cost of giving up exact diagonalization from the SNSS.sd method, which introduces more computational complexity as joint diagonalization algorithms need to be applied.

Both former methods have in common that only the spatial ordering of the sample locations is taken into account but not the spatial dependencies between them when computing the unmixing matrix. A trivial example which would cause problems is the case when the matrices $\boldsymbol{\Sigma}_{\mathbf{s}}$ are the identity matrix for all $\mathbf{s} \in \mathcal{S}$ but $\boldsymbol{\Sigma}_{\mathbf{s}\mathbf{s}'}$ is non-zero and spatial dependent. In that case the identifiability conditions of Definition 4 and consequently the one of Definition 3 do not hold and the two methods fail. In that case recovering the latent random field is still possible when considering second order spatial dependencies as suggested in the following approach.

3.3. Joint diagonalization of more than two local covariance matrices

The following SNSS.sjd divides the domain into at least two parts and jointly diagonalizes the corresponding local covariance matrices for a set of kernel functions, therefore, it utilizes second order spatial dependence (sjd).

Definition 5 (*SNSS.sjd Functional*)**.** Consider a random field $\mathbf{x}(\mathbf{s})$ following the SNSS model (Definition 1). Standardize $\mathbf{x}(\mathbf{s})$ by $\mathbf{x}^{st}(\mathbf{s}) = \mathbf{M}^{-1/2}_{\mathcal{S},f_0}(\mathbf{x}(\mathbf{s}))(\mathbf{x}(\mathbf{s}) - \mathbf{b})$ and partition the spatial domain $\mathcal{S}$ into $\mathcal{S}_1, \ldots, \mathcal{S}_K$ where $\mathcal{S}_m \cap \mathcal{S}_n = \emptyset$ for $m, n = 1, \ldots, K$ and $m \neq n$. For a set of spatial kernel functions

$\{f_1, \ldots, f_L\}$, $\mathbf{U}$ is an orthogonal $p \times p$ joint diagonalization matrix of the matrices $\mathbf{M}_{\mathcal{S}_k,f_l}(\mathbf{x}^{st}(\mathbf{s}))$ for all $k = 1, \ldots, K$ and $l = 1, \ldots, L$, which maximizes

$$\sum_{k=1}^{K}\sum_{l=1}^{L} \|\mathrm{diag}(\mathbf{U}\mathbf{M}_{\mathcal{S}_k,f_l}(\mathbf{x}^{st}(\mathbf{s}))\mathbf{U}^\top)\|_F^2. \tag{14}$$

Then, the SNSS.sjd functional is given as $\mathbf{W}(\mathbf{x}(\mathbf{s})) = \mathbf{U}\mathbf{M}^{-1/2}_{\mathcal{S},f_0}(\mathbf{x}(\mathbf{s}))$.

Again, as in the case of the SNSS.jd method, for a finite sample joint diagonalization approximate algorithms need to be used.

When setting the number of spatial kernel functions $L = 1$ and the resulting spatial kernel function to $f = f_0$, then the SNSS.sjd method reduces to the SNSS.jd method. If additionally the spatial domain is only divided into two parts and the transformation step is adapted accordingly, the SNSS.sjd method further reduces to the SNSS.sd method. In similar manner, if the choice of the spatial kernel functions is free but the domain is not partitioned, then the original SBSS method as introduced in Nordhausen et al. (2015) and Bachoc et al. (2020) is obtained.

Identifiability and affine equivariance results are given in the following proposition.

Proposition 3. *The SNSS.sjd functional defined in Definition 5 is*

(1) *identifiable iff for all pairs $i, j = 1, \ldots, p$ and $i \neq j$ there exists a pair k, l with $k \in \{1, \ldots, K\}$ and $l \in \{1, \ldots, L\}$ such that $(\mathbf{M}^{-1}_{\mathcal{S},f_0}(\mathbf{z}(\mathbf{s}))\mathbf{M}_{\mathcal{S}_k,f_l}(\mathbf{z}(\mathbf{s})))_{ii} \neq (\mathbf{M}^{-1}_{\mathcal{S},f_0}(\mathbf{z}(\mathbf{s}))\mathbf{M}_{\mathcal{S}_k,f_l}(\mathbf{z}(\mathbf{s})))_{jj}$,*

(2) *affine equivariant as seen in Definition 2.*

Proposition 3 is again more general than Proposition 2 as more kernel functions can be considered. The most general case is achieved when one member of the set of kernel functions $\{f_1, \ldots, f_L\}$ is f_0.

4. Simulations

In this part we investigate the performance of the different unmixing matrix estimators which are introduced beforehand in an extensive simulation study. All simulations are carried out in R version 3.6.1 (Team, 2019) with the help of the packages JADE (Miettinen et al., 2017), RandomFields (Schlather et al., 2015) and SpatialBSS (Muehlmann et al., 2021c), where the latter one contains functions for all introduced estimators.

4.1. Simulation settings and performance measure

We use always squared two-dimensional domains of the form $\mathcal{S} = [0, n] \times [0, n]$ (later denoted also as $n \times n$) where $n \in \{20, 30, 40, 50, 60, 70\}$. The set of sample locations $\mathcal{C}$ is formed by two different patterns, namely a uniform and skewed pattern. For the uniform coordinate pattern n^2 x and y values are sampled from the uniform distribution $U(0, 1)$ and then the sampled values are multiplied by n. The skewed coordinate pattern is formed by n^2 x values that are sampled from the beta distribution $\beta(2, 5)$ and n^2 y values that are sampled from the uniform distribution $U(0, 1)$, again all values are multiplied by n. This way of sampling coordinates ensures that the density of sample locations is the same for all domain sizes. In the case of the uniform pattern it equals one throughout the whole domain, whereas the skewed pattern shows more dense sample locations in the left half of the domain. Fig. 1 depicts one example for the uniform and skewed coordinate pattern for different domain sizes. As the qualitative meaning of the following simulations are equal for the uniform and the skewed setting we focus the subsequent discussions on the uniform setting and present the results for the skewed setting in the appendix.

Moreover, we randomly divide the spatial domain at hand into three different parts. This is done by randomly placing three locations on the spatial domain that act as cluster centers, which is depicted by the crosses ($\times$) in Fig. 1. The three clusters of sample locations are then determined by

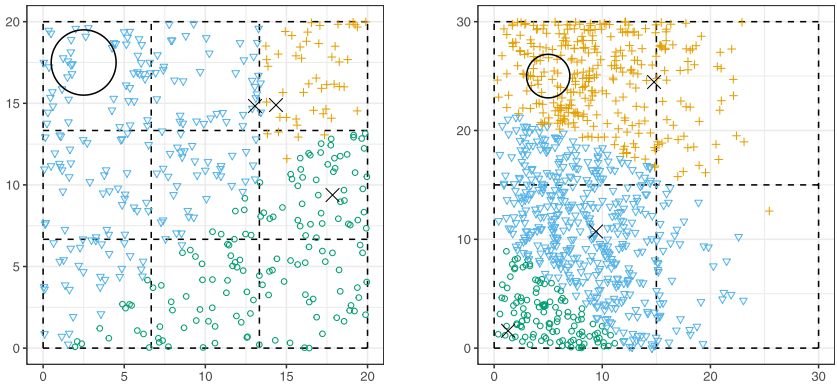

Fig. 1. Sample coordinates for a domain size of 20 × 20 of the uniform coordinate pattern (left) and for a domain size of 30 × 30 for the skewed coordinate pattern (right). The black crosses (×) depict the three randomly placed cluster centers, and the three different colors and shapes hint the corresponding clusters for the sample locations. The dashed lines depict different partitions of the spatial domain. The ring with radius two depicts the parameter used for the spatial kernel functions. (For interpretation of the references to color in this figure legend, the reader is referred to the web version of this article.)

the lowest Euclidean distance of the sample locations to the cluster centers, this is illustrated by the different colors and shapes for the sample locations in Fig. 1.

Using these locations we simulate random fields that follow in all but one setting the SNSS Model (Model 1). The dimension is set to $p = 3$ for all simulations. As our introduced methods are affine equivariant (as seen in Propositions 1–3) we choose without loss of generality $\mathbf{A} = \mathbf{I}_3$ and $\mathbf{b} = \mathbf{0}$ which determines $\mathbf{x}(\mathbf{s}) = \mathbf{z}(\mathbf{s})$. The six considered Gaussian distributed random field settings for the latent random field $\mathbf{z}(\mathbf{s})$ are as follows.

Setting 1. This setting is formed by iid Gaussian distributed 3-variate random vectors with different covariance matrices in each cluster of sample locations. $\boldsymbol{\Sigma}_{\mathbf{s}}$ equals diag(1, 3, 2) for cluster one, diag(2, 4, 2) for cluster two and diag(1, 3, 5) for cluster three. Thus, $\boldsymbol{\Sigma}_{\mathbf{ss}'} = \mathbf{0}$ for the whole spatial domain.

Setting 2 and 3. We sample in each coordinate cluster different random fields independently following the Matérn covariance function introduced in Section 1. In particular for Setting 2 the covariance function of $z_1(\mathbf{s})$, $C_{z_1}(h)$ equals $C(h; 1.0, 0.5, 0.5)$ for cluster 1, $C(h; 1.0, 1.0, 1.0)$ for cluster 2 and $C(h; 1.0, 1.0, 2.0)$ for cluster 3. $C_{z_2}(h)$ equals $C(h; 1.0, 1.5, 2.7)$ for cluster 1, $C(h; 1.0, 0.7, 1.0)$ for cluster 2 and $C(h; 1.0, 1.2, 1.9)$ for cluster 3. $C_{z_3}(h)$ equals $C(h; 1.0, 1.2, 1.4)$ for cluster 1, $C(h; 1.0, 0.5, 3.0)$ for cluster 2 and $C(h; 1.0, 0.7, 0.7)$ for cluster 3. Setting 3 is formed in the same fashion as Setting 2 with the only difference that the variance parameters are changed to the ones from Setting 1.

Setting 4 and 5. These settings are based on the non-stationary extension of the Matérn covariance function presented in Anderes and Stein (2011) given by

$$
\begin{aligned}
C(\mathbf{s}, \mathbf{s}'; \sigma, \nu, \phi) &= \sigma(\mathbf{s})\sigma(\mathbf{s}') \left(\frac{\phi^2(\mathbf{s})/4\nu(\mathbf{s})}{\Gamma(\nu(\mathbf{s}))2^{\nu(\mathbf{s})-1}} \right)^{1/2} \left(\frac{\phi^2(\mathbf{s}')/4\nu(\mathbf{s}')}{\Gamma(\nu(\mathbf{s}'))2^{\nu(\mathbf{s}')-1}} \right)^{1/2} \\
&\left(\frac{\phi^2(\mathbf{s})}{8\nu(\mathbf{s})} + \frac{\phi^2(\mathbf{s}')}{8\nu(\mathbf{s}')} \right)^{-1} \left\| \tilde{\mathbf{h}} \right\|^{(\nu(\mathbf{s})+\nu(\mathbf{s}'))/2} K_{(\nu(\mathbf{s})+\nu(\mathbf{s}'))/2} \left(\left\| \tilde{\mathbf{h}} \right\| \right), \qquad (15) \\
\tilde{\mathbf{h}} &= \left(\frac{\phi^2(\mathbf{s})}{8\nu(\mathbf{s})} + \frac{\phi^2(\mathbf{s}')}{8\nu(\mathbf{s}')} \right)^{-1/2} (\mathbf{s} - \mathbf{s}'),
\end{aligned}
$$

where K_ν is the modified Bessel function of second kind, $\sigma^2 : \mathcal{S} \to \mathbb{R}^+$, $\nu : \mathcal{S} \to \mathbb{R}^+$ and $\phi : \mathcal{S} \to \mathbb{R}^+$ are the local variance, shape and range parameter functions. We choose these functions to be of the form $g(\mathbf{x}) = \sum_{i=1}^{3} c_i \mathbf{1}(\mathbf{x} \in \mathcal{C}_i)$, where $\mathcal{C}_i$ are the three clusters of sample locations as defined above. The c_i coefficients are the same as the ones from the independently sampled random fields of Setting 2 and 3 for Setting 4 and 5 respectively.

Setting 6. Setting 6 is a stationary SBSS setting, where the entries of the latent field are following a Matérn covariance function. Explicitly, $C_{z_1}(h)$ equals $C(h; 1.0, 0.5, 1.0)$, $C_{z_2}(h)$ equals $C(h; 1.0, 1.0, 1.5)$ and $C_{z_3}(h)$ equals $C(h; 1.0, 1.5, 2.0)$.

Note that Setting 1 can be viewed as different white noise for the different clusters of sample locations. For Setting 2 and 3 the random fields are independent between clusters which is not the case for Setting 4 and 5. Setting 2 and 4 have a global constant variance of 1 for all entries of the random field, whereas in Setting 3 and 5 also the variances are different in each cluster of sample locations. Setting 6 is globally stationary with constant variance for each entry of the latent random field. Thus, Setting 6 does not really fit into the SNSS framework but rather into the SBSS framework.

To evaluate the quality of the unmixing matrix estimate $\hat{\mathbf{W}}$ from the different methods we use the minimum distance index (MDI) (Ilmonen et al., 2010; Lietzen et al., 2020) which is defined as

$$\text{MDI}(\hat{\mathbf{W}}\mathbf{A}) = \frac{1}{\sqrt{p-1}} \inf_{\mathbf{J} \in \mathcal{J}} \|\mathbf{J}\hat{\mathbf{W}}\mathbf{A} - \mathbf{I}_p\|_F. \tag{16}$$

Here, $\mathcal{J}$ is the set of all matrices that carry exactly one non-zero element in each row and column which corresponds to all matrices of the form **PSD** that are exactly the indeterminacies of our model definition. The MDI is a function $\text{MDI} : \mathbb{R}^{p \times p} \to [0, 1]$ where zero indicates that the estimated unmixing matrix meets exactly the real one up to scale, sign and permutation of its rows and one indicates a very poor estimate.

4.2. Comparison to contender methods

For this part of the simulations we estimate the unmixing matrix $\hat{\mathbf{W}}$ with all SNSS methods described above. For the SNSS.sd method given by Definition 3 we divide the domain in half across the coordinate x axis (SNSS.sd x) and the coordinate y axis (SNSS.sd y). For the SNSS.jd method seen in Definition 4 and SNSS.sjd given by Definition 5 we define the sub-domains by dividing the domain at hand in four equal squared blocks as shown on the right panel of Fig. 1. Additionally, for the SNSS.sjd method we use a ring kernel with $(r_1, r_2) = (0, 2)$ and f_0 (SNSS.sjd). This choice keeps the average number of sample locations at $r^2\pi \approx 12$ for the uniform setting. As contender methods we estimate the unmixing matrix with the SBSS method, introduced in Nordhausen et al. (2015) and Bachoc et al. (2020), with the same spatial kernel function settings as before but without f_0 (SBSS). Lastly, we use the fourth order blind identification (FOBI) method which is a popular independent component analysis (ICA) method that does not utilize spatial information but fourth order cumulants, see Cardoso (1989) and Nordhausen and Virta (2019).

The average MDI based on 2000 simulation iterations for the above estimators for all six considered random field models are presented in Fig. 2 for the uniform sample location pattern. As in Setting 1 the random field shows no spatial dependence all SBSS methods completely fail as they only rely on spatial dependencies and the SNSS.jd method outperforms all contender methods. SNSS.sd is inferior which might be explained by the fact that it only halves the spatial domain, whereas SNSS.jd uses four equally sized sub-domains. Even though the SNSS.sjd methods use the sample covariance matrix inside each sub-domain, additionally (non-informative) local covariance matrices are used which might bring noise into the joint diagonalization algorithm and therefore reduce its performance in this setting. In contrast to Setting 1 only methods that rely on spatial dependencies perform well in Setting 2 and 4 as the variance for this setting equals one for each entry of the random field globally. Interestingly, the SBSS methods still perform well in Setting 2, this might result from the fact that this Setting is based on stationary covariance functions. In Setting 4 SBSS is clearly outperformed by the SNSS.sjd method. As the covariance is non-constant for Setting 3 and 5 also the SNSS.sd and SNSS.jd methods improve their performance compared to Setting 2

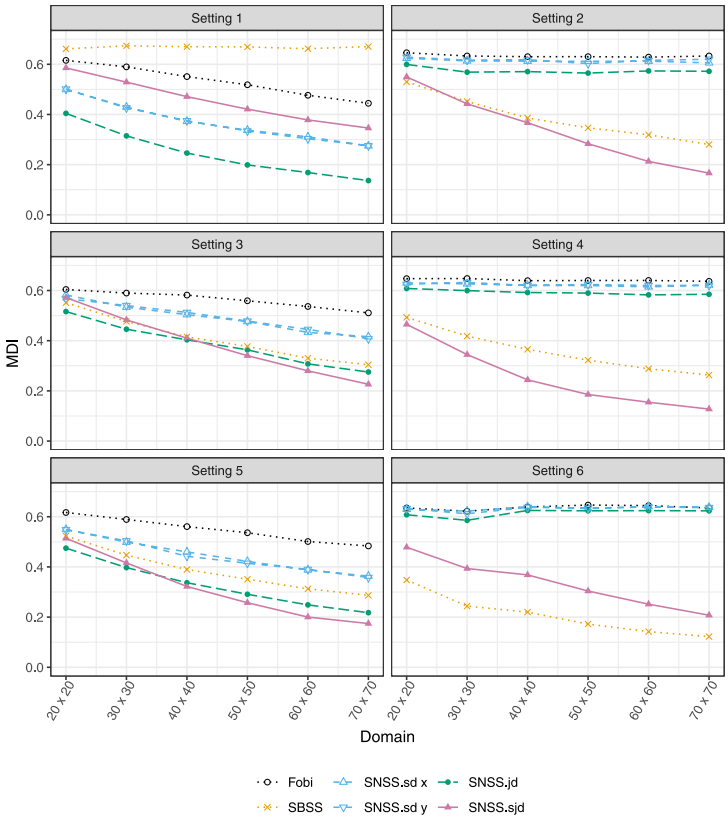

Fig. 2. Average MDI based on 2000 simulation repetitions for all random field models, different estimators and sample sizes for the uniform sample location pattern.

and 4 where the covariance is constant. Lastly, as Setting 6 is formed by stationary latent fields with global constant variances (namely a SBSS model), only the SBSS and the SNSS.sjd are expected to deliver meaningful results. However, SBSS shows a better performance because the domain is not split into parts, therefore the effective sample size for the local covariance estimation is higher leading to a better separation. Interestingly, for all simulations where the variance is non-constant FOBI increases its performance as the sample size increases. The impact of different kernel function settings and domain subdivisions is studied in the subsequent part.

4.3. Different domain subdivisions

The former simulations are carried out for a fixed partition of the spatial domain for the SNSS.jd and SNSS.sjd methods. In this part we investigate the influence of different partitions on the overall performance of the unmixing matrix estimation. We consider sub-divisions into four (2×2), nine (3×3) and 16 (4×4) equally sized squared blocks for both methods. Exemplary, 3×3 is depicted on the left panel and 2×2 is depicted on the right panel of Fig. 1. Additionally, we half the domain across the x and the y axes for the SNSS.sjd method. The spatial kernel function settings equal the ones from the former simulations. The mean MDIs based on 2000 simulation repetitions are shown in Fig. 3 for the uniform sample location pattern. Overall, the influence of the domain sub-division is very minor except for the SNSS.sjd method in Setting 1 and 6. Again, in Setting 6 the performance increases as the sub-division of the domain decreases, and more information is available to estimate

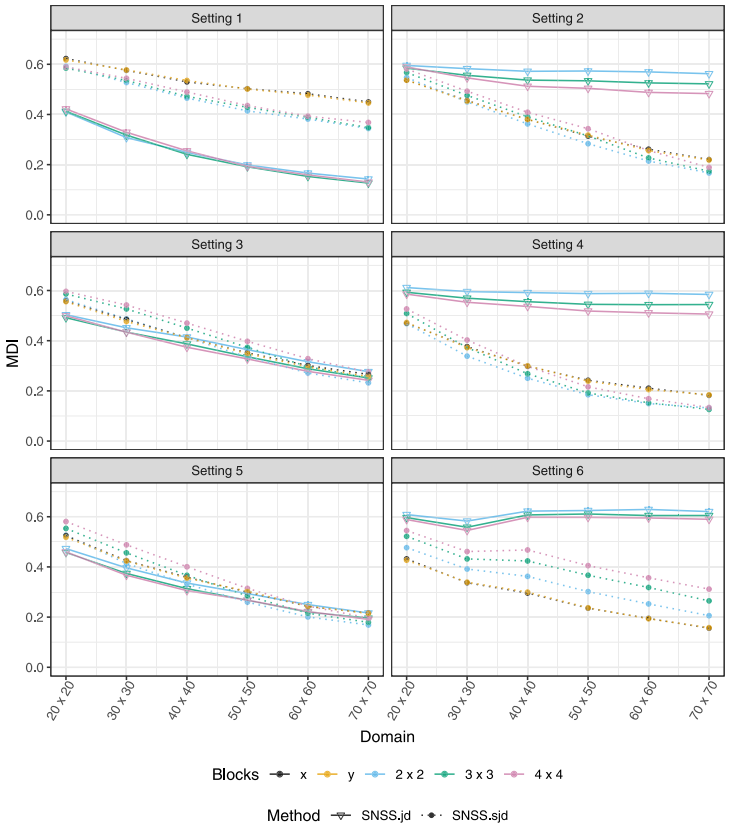

Fig. 3. Average MDI based on 2000 simulation repetitions for all random field models, different block sub-domain structures for the SNSS.jd and SNSS.sjd methods and sample sizes for the uniform sample location pattern.

the matrices of interest. The optimal case is given when the domain is not divided at all, which leads to the original SBSS method.

4.4. Different kernel functions

In the last part of the simulations we investigate the influence of different kernel function settings on the performance of the SBSS and the SNSS.sjd methods. For the SNSS.sjd method we again quarter the domain as before. For the kernel settings we consider a ball and a Gauss kernel with the parameter $r = 2$ and a ring kernel with the parameter $(r_1, r_2) = (0, 2)$ denoted as B(2), G(2), R(0,2) respectively. Additionally, for the SNSS.sjd method we use the covariance per sub-domain f_0 or do not use it (denoted as SNSS.sjd w/c and SNSS.sjd wo/c respectively). The average MDI based on 2000 simulation iterations for these simulations are depicted in Fig. 4. The choice of the kernel function setting does not seem to be of great influence for the settings with spatial dependence (Setting 2 - Setting 6). For Setting 1 constituted of different iid samples in the clusters it is interesting to see that SBSS and SNSS.sjd without f_0 and a ring kernel fail. The latter is due to the fact that f_0 is absent and the ring kernel does not account for on-site variance which in total leads to a method that separates the signal by only relying on spatial dependence. But, Setting 1 does not exhibit spatial dependence resulting in meaningless results for this method/kernel combination.

Generally, the simulation study shows that SNSS.sjd might be the favorable method as it always improves its performance with increasing sample size which reflects its ability to deliver meaningful

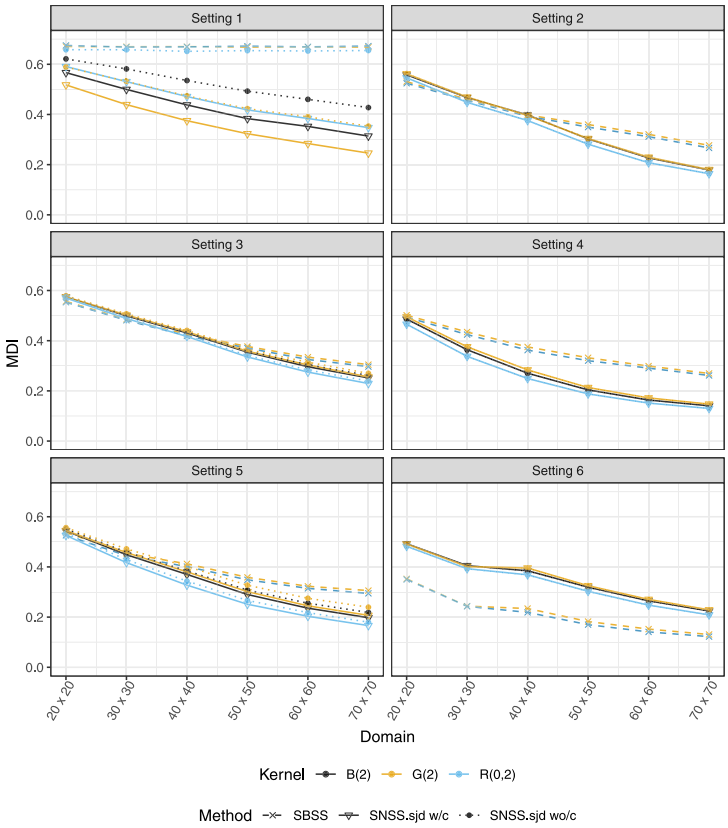

Fig. 4. Average MDI based on 2000 simulation repetitions for all random field models, different kernel functions for the SBSS and SNSS.sjd methods and sample sizes for the uniform sample location pattern.

results in a broad range of applications. Its performance is never among the last and it is among the best in four out of six simulation settings which hints that it might be the go-to choice when the underlying structure of the data is unclear. Surprisingly, the original SBSS method shows good performance in almost all settings with overall best performance when the SBSS model holds true but worst performance when all the information is only present in on-site variance. In the following, we investigate the usefulness of the SNSS.sjd method on a real data example.

5. Data example

In this section we illustrate the use of the above introduced methods on an environmental application. Specifically, we consider a dataset that is derived from the GEMAS geochemical mapping project (Reimann et al., 2014) which consists of concentration measurements of 18 elements (Al, Ba, Ca, Cr, Fe, K, Mg, Mn, Na, Nb, P, Si, Sr, Ti, V, Y, Zn, Zr) in 2017 agricultural soil samples. This dataset is freely available in the R package robCompositions (Filzmoser et al., 2018).

As it is common practice in geochemical applications we respect the relative information of the data by performing typical compositional data analysis transformations prior the actual SNSS analysis. In a BSS context this is for example discussed in Muehlmann et al. (2021a) and Nordhausen et al. (2015) and we follow in the exact same fashion as outlined in Nordhausen et al. (2015). We first perform an isometric log-ratio (ilr) transformation by using pivot coordinates, and then apply the SNSS method. The loadings matrix is formed by combining the contrast matrix and the estimated

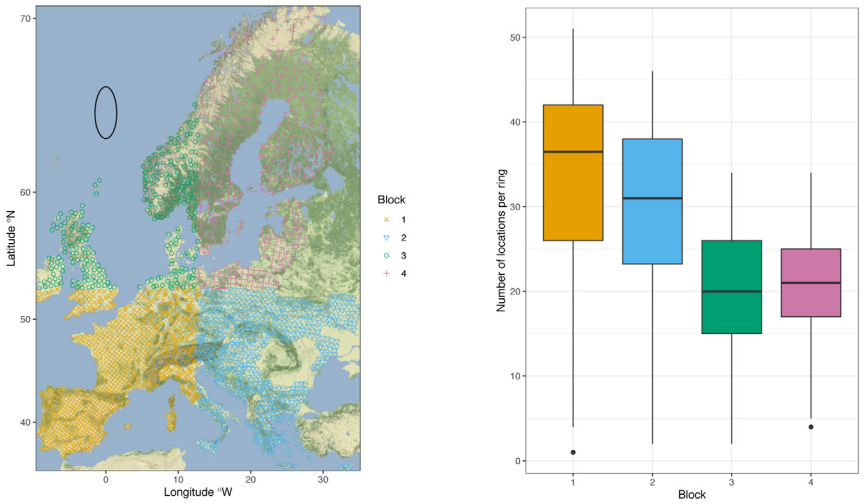

Fig. 5. Sample locations for the GEMAS dataset (left panel). The four different colors and shapes illustrate the sub-division of the spatial domain into four equally shaped rectangular blocks. Blocks one to four contain 720, 654, 258 and 475 sample locations respectively. The ring of radius 1.5° depicts the parameter choice for the ring kernel function. Number of considered neighboring sample locations defined by the ring kernel choice for each of the four blocks (right panel). Map tiles by Stamen Design, under CC BY 3.0. Data by OpenStreetMap, under ODbL. (For interpretation of the references to color in this figure legend, the reader is referred to the web version of this article.)

unmixing matrix. Here the contrast matrix is an orthogonal matrix that transforms the data from centered log-ratio (clr) into ilr coordinates. Details on clr, ilr and compositional data analysis in general are given for example in Aitchison (2003). Note that the ilr transformation reduces the dimension of the dataset by one, therefore $p = 17$.

We carry out the analysis with the SNSS.sjd method as it makes the overall best impression in the simulation study. We divide the domain into four equally sized rectangles where the four resulting blocks of sample locations are depicted in the left panel of Fig. 5. The circle on that Figure illustrates the parameter $(r_1, r_2) = (0°, 1.5°)$ for the used ring kernel function and the right panel of Fig. 5 shows boxplots of the number of neighboring sample locations defined by the ring kernel choice for each of the four considered blocks of sample locations. Additional to the ring kernel function choice we also include the covariance matrix for each of the four blocks (kernel function f_0). Fig. 6 depicts the variograms of all component of the ilr data computed for each of the four blocks individually. Clearly, all panels show strong differences for each sub-domain indicating the non-stationarity of the data at hand.

We compute moving block variance maps for each entry of the latent random field. Specifically, we overlaid the domain by a grid with a resolution of one degree where the center is placed on the minimum longitude and latitude value present in the dataset. The variance for each cell of the grid is computed by considering all sample locations that lie inside a block of size $3° \times 3°$ that is placed on that cell.

After visual inspection of all recovered entries of the latent random field and the corresponding moving block variance maps we exemplary present the first two entries in Figs. 7 and 8. The corresponding combined loadings (matrix product of the contrast and the estimated unmixing matrix) that transform the clr data into the first and second entry of the latent random field are presented in Table 1. A cluster of high values for the first component of the latent random field is found on the Iberian Peninsula. This cluster is mostly formed by the high balance between the pair Al, Ti and Na, V as the corresponding loadings show roughly equal values with opposite signs. The second component of the latent random field shows a cluster of high variance as well as high values in Greece, along the Balkan up to the northern and central part of Italy. The high loading

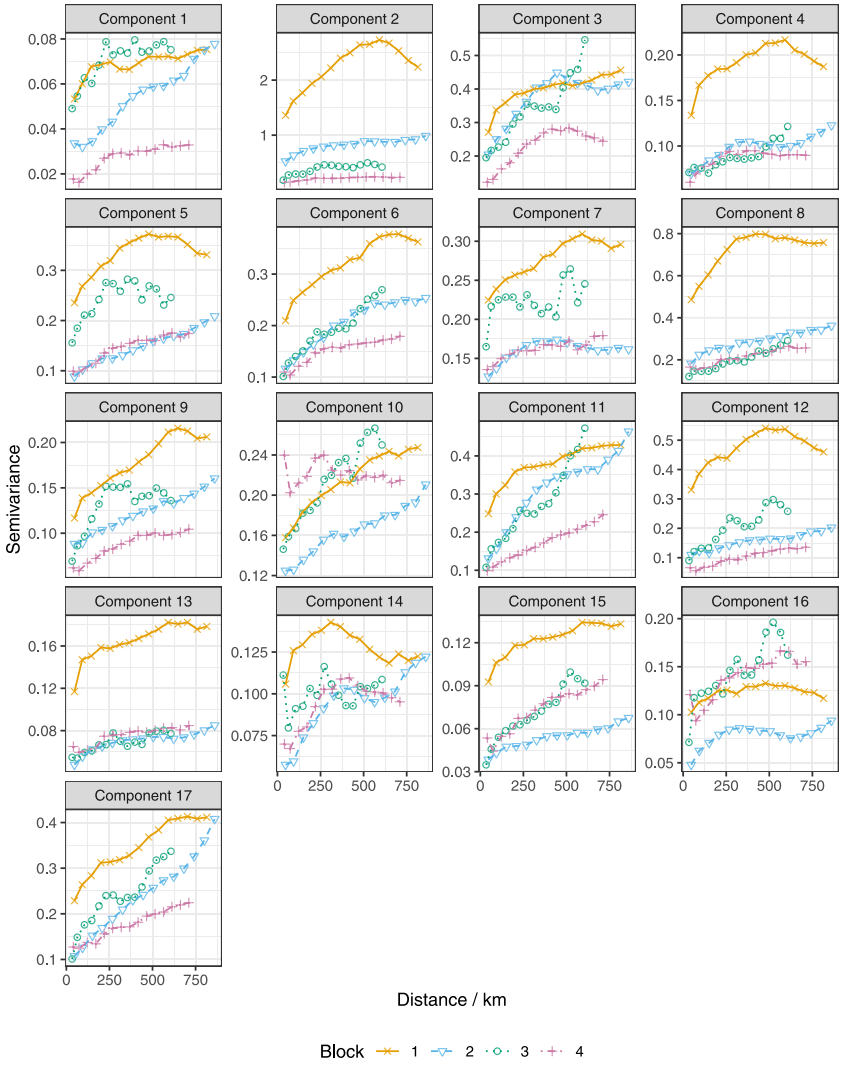

Fig. 6. Sample variograms of all components of the ilr data individually computed for each sub-domain defined by the left panel of Fig. 5. Note that the maximum distance is different for each sample variogram as it is chosen to be a third of the diagonal of the smallest rectangle containing the sample locations.

of clr(Al) and the roughly equal absolute values of the clr(Cr) and clr(Zr) loadings suggest that this entry is mostly driven by a positive log-ratio between Cr and Zr combined with the high relative dominance of Al. The opposite effect is observed for the cluster of low values from mid to east Europe and the southern part of Scandinavia. Deeper investigation of the found latent random field and the possible driving physical phenomena can be achieved by geological experts. The moving block variance maps show a non-constant variance for all found components of the latent field. This again hints the non-stationarity of the data as it is highly likely that linear combinations of the non-stationary latent components (which are the observable random fields) are non-stationary.

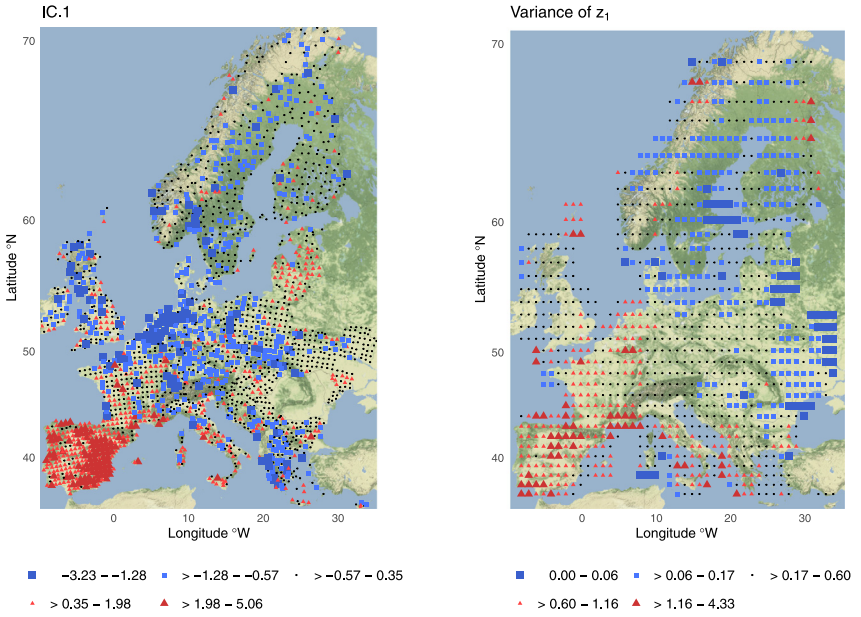

Fig. 7. Map of the first entry of the estimated latent field (left) and its corresponding moving block variance map (right). Map tiles by Stamen Design, under CC BY 3.0. Data by OpenStreetMap, under ODbL.

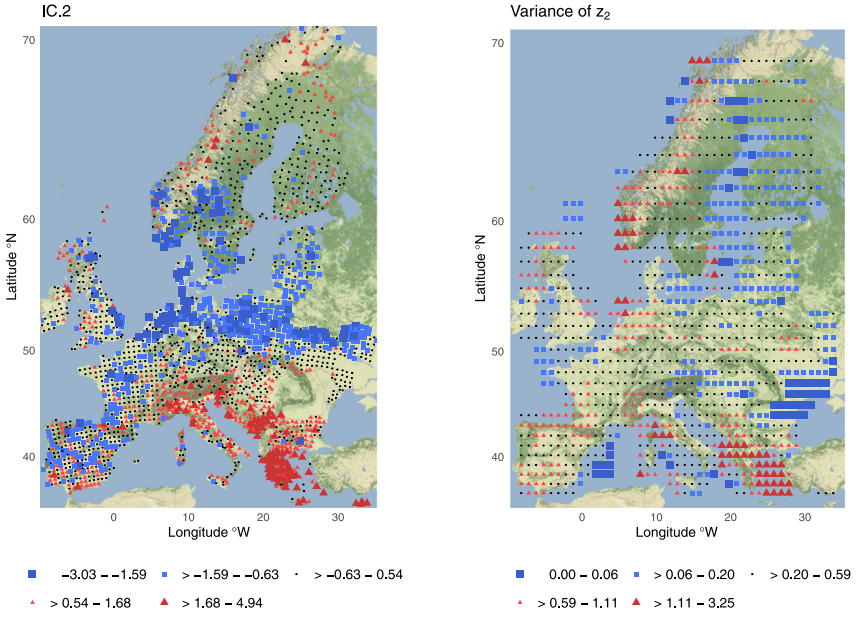

Fig. 8. Map of the second entry of the estimated latent field (left) and its corresponding moving block variance map (right). Map tiles by Stamen Design, under CC BY 3.0. Data by OpenStreetMap, under ODbL.

Table 1
Values of the combined loadings matrix that transforms the clr data into the first two components of the estimated latent random field.

	z_1	z_2		z_1	z_2
clr(Al)	**1.72**	**1.47**	clr(Nb)	−0.50	0.02
clr(Ba)	−0.23	−0.29	clr(P)	−0.15	−0.40
clr(Ca)	0.06	0.09	clr(Si)	0.71	−0.32
clr(Cr)	−0.55	**1.01**	clr(Sr)	0.42	−0.15
clr(Fe)	0.86	−0.18	clr(Ti)	**1.38**	−0.12
clr(K)	0.13	−0.27	clr(V)	**−1.29**	−0.68
clr(Mg)	0.30	−0.17	clr(Y)	−0.05	0.53
clr(Mn)	−0.36	0.26	clr(Zn)	−0.60	−0.06
clr(Na)	**−1.22**	0.18	clr(Zr)	−0.63	**−0.91**

To illustrate the usefulness of the SNSS methods as a data pre-processing tool for spatial prediction tasks we conclude this section by discussing a possible three-step prediction blueprint as follows.

Step 1: One of the formerly introduced SNSS methods is applied on the data to estimate the unmixing matrix $\hat{\mathbf{W}}$ and the latent random field $\hat{\mathbf{z}}(\mathbf{s}) = (\hat{z}_1(\mathbf{s}), \ldots, \hat{z}_p(\mathbf{s}))^\top$.

Step 2: As all entries of $\hat{\mathbf{z}}$ are uncorrelated, each entry can be predicted individually on an unobserved location $\mathbf{s}^*$ by any spatial prediction method available. Preferably a method that meets the constant drift and non-stationarity assumptions of the latent field components.

Step 3: The individual predictions from Step 2 are collected again into a vector $\hat{\mathbf{z}}(\mathbf{s}^*) = (\hat{z}_1(\mathbf{s}^*), \ldots, \hat{z}_p(\mathbf{s}^*))^\top$. The prediction of the original data is formed by mixing the predicted latent vector with the quantities estimated in Step 1 leading to $\hat{\mathbf{x}}(\mathbf{s}^*) = \hat{\mathbf{W}}^{-1}\hat{\mathbf{z}}(\mathbf{s}^*) + \hat{\mathbf{T}}(\mathbf{x}(\mathbf{s}))$, where $\hat{\mathbf{T}}(\mathbf{x}(\mathbf{s}))$ is an estimator of the used location functional.

This procedure is especially appealing as only univariate models need to be defined and fitted in Step 2. Hence, the estimation and modeling of cross dependencies is completely discarded. For the SBSS model and estimators Muehlmann et al. (2021d) outline and compare this approach with multivariate prediction methods in an extensive simulation study and on a geochemical application.

6. Conclusion

BSS has been successfully used in many scientific applications (Comon and Jutten, 2010). It has a long tradition for iid data where it is known as independent component analysis (ICA) and for stationary and non-stationary time series (Pan et al., 2021). Recently, BSS approaches were suggested for stationary spatial data (Nordhausen et al., 2015; Bachoc et al., 2020). In this paper, we combine ideas from non-stationary time series methods and spatial stationary BSS to develop approaches for non-stationary spatial data. We formulate a spatial non-stationary blind source separation model and provide three different estimators that are based on the joint diagonalization of covariance and local covariance matrices for sub-divisions of the spatial domain. These estimators can be easily applied on spatial datasets with irregular sample locations and their use is illustrated in an extensive simulation study and on an environmental application.

Interesting future research would be to derive asymptotic results for the different estimators. Furthermore, it is of great interest to explore the use of the SNSS methods in the context of spatial prediction. The entries of the latent random field are uncorrelated, therefore, p univariate non-stationary models can be built which is much simpler as building one multivariate model for the original data. In the stationary case, such an approach seemed promising as discussed in Muehlmann et al. (2021d). Another interesting question would be to test if all latent components are actually informative and non-stationary, perhaps some exhibit spatial dependence but are stationary and others might be just white noise. In such cases modeling could be simplified. The separation of

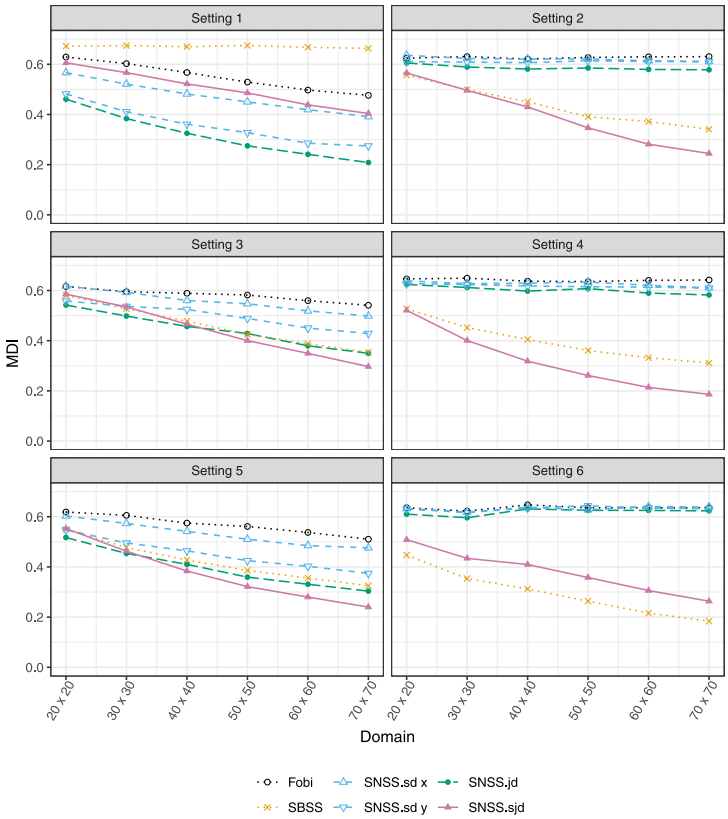

Fig. B.9. Average MDI based on 2000 simulation repetitions for all random field models, different estimators and sample sizes for the skewed sample location pattern. See Section 4.2 for details.

stationary from white noise processes in SBSS is for example discussed in Muehlmann et al. (2020). Lastly, the introduced SNSS methods need a subdivision of the spatial domain at hand a priory. As the optimal number and shapes of the sub-domains are not clear we focus our discussion on different numbers of rectangular sub-domains which show good performance in the simulation study. One theoretical argument is given by the identifiability conditions which loosely state that the (spatial) second-order dependencies of the latent fields need to be as different as possible across the sub-domains to ensure optimal signal separation. However, as the latent fields are unknown in the first place the practical use of this statement is limited and interesting future research might be to find more practical rules for choosing the domain subdivision.

In a time series context Pfister et al. (2019) viewed such a partition of the data as a realization of grouped data and adapted the BSS model to such a case. A motivating example would be Electroencephalography (EEG) signals where the sensors are placed on the same locations for different patients ensuring the same way of mixing. The measurements for each patient then form the different groups. However, motivation for the adaptation to the spatial setting is a future problem.

Acknowledgment

Funding: This work was supported by the Austrian Science Fund [grant numbers P31881-N32]. The authors thank the editors and referees for helpful and insightful comments and suggestions that greatly improved the manuscript.

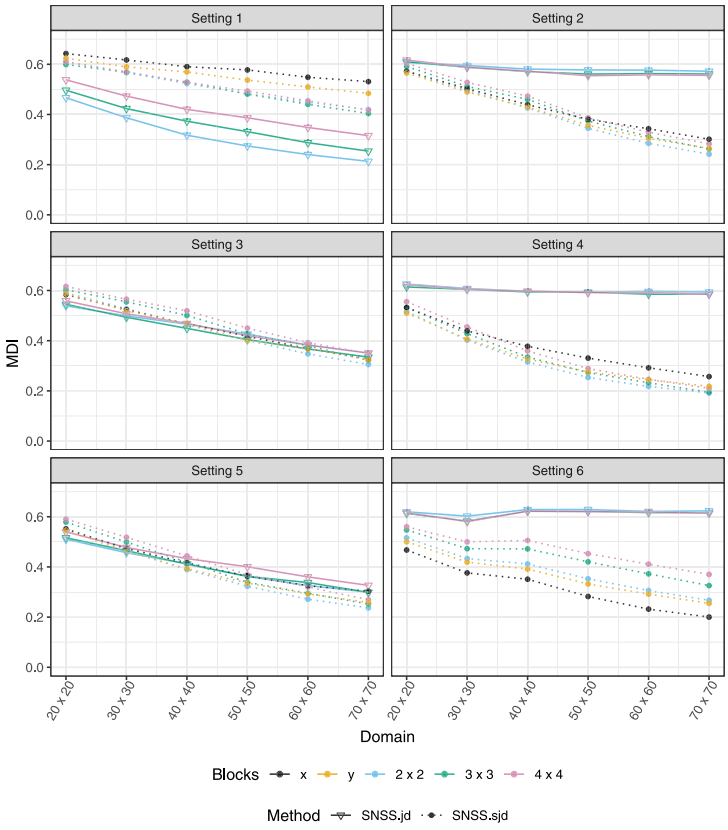

Fig. B.10. Average MDI based on 2000 simulation repetitions for all random field models, different block sub-domain structures for the SNSS.jd and SNSS.sjd methods and sample sizes for the skewed sample location pattern. See Section 4.3 for details.

Appendix A. Proof of the propositions

Proof of Proposition 1. Identifiability: For a given simultaneous diagonalizer $\mathbf{W}$ the first optimization equation writes

$$\begin{aligned}\mathbf{I}_p &= \mathbf{W}\mathbf{M}_{\mathcal{S}_1,f_0}(\mathbf{x}(\mathbf{s}))\mathbf{W}^\top = \mathbf{W}\mathbf{A}\mathbf{A}^{-1}\mathbf{M}_{\mathcal{S}_1,f_0}(\mathbf{x}(\mathbf{s}))\mathbf{A}^{-\top}\mathbf{A}^\top\mathbf{W}^\top \\ &= \mathbf{W}\mathbf{A}\mathbf{M}_{\mathcal{S}_1,f_0}(\mathbf{z}(\mathbf{s}))\mathbf{A}^\top\mathbf{W}^\top.\end{aligned} \tag{A.1}$$

As $\mathbf{M}_{\mathcal{S}_1,f_0}(\mathbf{z}(\mathbf{s}))$ is a diagonal matrix with strictly positive diagonal elements by assumption it follows that $\mathbf{W}\mathbf{A}\mathbf{M}^{1/2}_{\mathcal{S}_1,f_0}(\mathbf{z}(\mathbf{s})) = \mathbf{V}$ where $\mathbf{V}$ is a $p \times p$ orthogonal matrix. With that the second optimization equations write as

$$\mathbf{D}_{\mathcal{S}_1\mathcal{S}_2} = \mathbf{W}\mathbf{A}\mathbf{M}_{\mathcal{S}_2,f_0}(\mathbf{z}(\mathbf{s}))\mathbf{A}^\top\mathbf{W}^\top = \mathbf{V}\mathbf{M}^{-1}_{\mathcal{S}_1,f_0}(\mathbf{z}(\mathbf{s}))\mathbf{M}_{\mathcal{S}_2,f_0}(\mathbf{z}(\mathbf{s}))\mathbf{V}^\top. \tag{A.2}$$

$\Leftarrow$: As the diagonal elements of the matrix $\mathbf{M}^{-1}_{\mathcal{S}_1,f_0}(\mathbf{z}(\mathbf{s}))\mathbf{M}_{\mathcal{S}_2,f_0}(\mathbf{z}(\mathbf{s}))$ are pairwise distinct the matrix $\mathbf{D}_{\mathcal{S}_1\mathcal{S}_2}$ has p unique one-dimensional eigenspaces that are orthogonal. Therefore, $\mathbf{V}$ can only be of the form $\mathbf{PS}$, and hence $\mathbf{WA} = \mathbf{PSM}_{\mathcal{S}_1,f_0}(\mathbf{z}(\mathbf{s}))^{-1/2}$ which is of the form $\mathbf{PSD}$.

$\Rightarrow$: Assume w.l.o.g. that the first two diagonal elements of $\mathbf{M}^{-1}_{\mathcal{S}_1,f_0}(\mathbf{z}(\mathbf{s}))\mathbf{M}_{\mathcal{S}_2,f_0}(\mathbf{z}(\mathbf{s}))$ are equal, denoted as λ. Then from the second optimization equation the first two eigenvalue equations write $\mathbf{D}_{\mathcal{S}_1\mathcal{S}_2}\mathbf{v}_1 = \mathbf{v}_1\lambda$ and $\mathbf{D}_{\mathcal{S}_1\mathcal{S}_2}\mathbf{v}_2 = \mathbf{v}_2\lambda$ where the eigenvectors can be written as $\mathbf{v}_1 =$

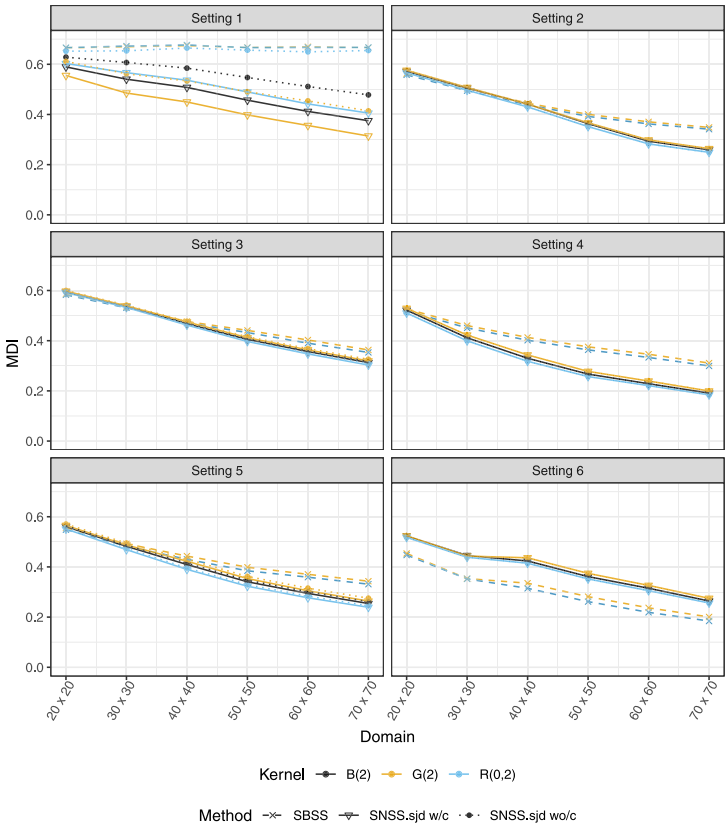

Fig. B.11. Average MDI based on 2000 simulation repetitions for all random field models, different kernel functions for the SBSS and SNSS.sjd methods and sample sizes for the skewed sample location pattern. See Section 4.4 for details.

$(1/\sqrt{2}, 1/\sqrt{2}, 0, \ldots, 0)^\top$ and $\mathbf{v}_2 = (1/\sqrt{2}, -1/\sqrt{2}, 0, \ldots, 0)^\top$. But then $\mathbf{V}$ is not of the form $\mathbf{PS}$ and consequently $\mathbf{WA}$ is not of the form $\mathbf{PSD}$.

Affine equivariance: Consider an affine transformation of $\mathbf{x}(\mathbf{s})$ written as $\mathbf{x}^*(\mathbf{s}) = \mathbf{B}\mathbf{x}(\mathbf{s}) + \mathbf{a}$, where $\mathbf{B}$ is an invertible $p \times p$ matrix. The unmixing matrix functional $\mathbf{W}^* = \mathbf{W}^*(\mathbf{x}^*(\mathbf{s}))$ satisfies

$$\mathbf{W}^*\mathbf{M}_{\mathcal{S}_1,f_0}(\mathbf{x}^*(\mathbf{s}))\mathbf{W}^{*\top} = \mathbf{I}_p, \mathbf{W}^*\mathbf{M}_{\mathcal{S}_2,f_0}(\mathbf{x}^*(\mathbf{s}))\mathbf{W}^{*\top} = \mathbf{D}^*_{\mathcal{S}_1\mathcal{S}_2}, \tag{A.3}$$

for a diagonal matrix $\mathbf{D}^*_{\mathcal{S}_1\mathcal{S}_2}$. But because of the affine equivariance of local covariance matrices it also follows that

$$\mathbf{W}^*\mathbf{B}\mathbf{M}_{\mathcal{S}_1,f_0}(\mathbf{x}(\mathbf{s}))\mathbf{B}^\top\mathbf{W}^{*\top} = \mathbf{I}_p, \mathbf{W}^*\mathbf{B}\mathbf{M}_{\mathcal{S}_2,f_0}(\mathbf{x}(\mathbf{s}))\mathbf{B}^\top\mathbf{W}^{*\top} = \mathbf{D}^*_{\mathcal{S}_1\mathcal{S}_2}. \tag{A.4}$$

From the last equations $\mathbf{W}^*\mathbf{B}$ can be identified as the unmixing matrix $\mathbf{W}(\mathbf{x}(\mathbf{s}))$, this leads to $\mathbf{W}^*(\mathbf{x}^*(\mathbf{s})) = \mathbf{W}(\mathbf{x}(\mathbf{s}))\mathbf{B}^{-1}$ which concludes the proof. □

Proof of Proposition 2. Definition 4 is a special case of Definition 5, therefore, the proof of Proposition 2 is a special case of the proof of Proposition 3 for $L = 1$. □

Proof of Proposition 3. Identifiability: For a given unmixing matrix $\mathbf{W} = \mathbf{U}\mathbf{M}_{\mathcal{S},f_0}^{-1/2}(\mathbf{x}(\mathbf{s}))$ from the transformation step it follows that

$$\begin{aligned}\mathbf{I}_p &= \mathbf{U}\mathbf{I}_p\mathbf{U}^\top = \mathbf{U}\mathbf{M}_{\mathcal{S},f_0}^{-1/2}(\mathbf{x}(\mathbf{s}))\mathbf{M}_{\mathcal{S},f_0}(\mathbf{x}(\mathbf{s}))\mathbf{M}_{\mathcal{S},f_0}^{-1/2}(\mathbf{x}(\mathbf{s}))\mathbf{U}^\top \\ &= \mathbf{W}\mathbf{A}\mathbf{M}_{\mathcal{S},f_0}(\mathbf{z}(\mathbf{s}))\mathbf{A}^\top\mathbf{W}^\top.\end{aligned} \tag{A.5}$$

As $\mathbf{M}_{\mathcal{S},f_0}(\mathbf{z}(\mathbf{s}))$ is a diagonal matrix with strictly positive diagonal elements by assumption it follows that $\mathbf{W}\mathbf{A}\mathbf{M}_{\mathcal{S},f_0}^{1/2}(\mathbf{z}(\mathbf{s})) = \mathbf{V}$ where $\mathbf{V}$ is a $p \times p$ orthogonal matrix. From the maximization equation it follows that

$$\begin{aligned}&\sum_{k=1}^{K}\sum_{l=1}^{L}\|\mathrm{diag}(\mathbf{U}\mathbf{M}_{\mathcal{S}_k,f_l}(\mathbf{x}^{st}(\mathbf{s})))\mathbf{U}^\top\|_F^2 \\ &= \sum_{k=1}^{K}\sum_{l=1}^{L}(\|\mathbf{U}\mathbf{M}_{\mathcal{S}_k,f_l}(\mathbf{x}^{st}(\mathbf{s}))\mathbf{U}^\top\|_F^2 - \|\mathrm{off}(\mathbf{U}\mathbf{M}_{\mathcal{S}_k,f_l}(\mathbf{x}^{st}(\mathbf{s})))\mathbf{U}^\top\|_F^2),\end{aligned} \tag{A.6}$$

here $\mathrm{off}(\cdot)$ is obtained by setting all off-diagonal elements of the squared-matrix argument to zero. We have $\mathbf{M}_{\mathcal{S},f_0}^{-1/2}(\mathbf{x}(\mathbf{s})) = \mathbf{O}\mathbf{M}_{\mathcal{S},f_0}^{-1/2}(\mathbf{z}(\mathbf{s}))\mathbf{A}^{-1}$, with a unique orthogonal matrix $\mathbf{O}$, from Ilmonen et al. (2012, Theorem 2.1). Hence, one can show that there is an orthogonal matrix $\mathbf{U}'$ such that $\mathbf{U}'\mathbf{M}_{\mathcal{S}_k,f_l}(\mathbf{x}^{st}(\mathbf{s}))\mathbf{U}'^\top$, $k = 1,\dots,K$, $l = 1,\dots,L$ are diagonal (see the equivariance proof below). As $\mathbf{U}$ maximizes the sum of Frobenius norms of the diagonals we have that $\mathbf{U}\mathbf{M}_{\mathcal{S}_k,f_l}(\mathbf{x}^{st}(\mathbf{s}))\mathbf{U}^\top$, $k = 1,\dots,K$, $l = 1,\dots,L$ are diagonal. But also

$$\mathbf{U}\mathbf{M}_{\mathcal{S}_k,f_l}(\mathbf{x}^{st}(\mathbf{s}))\mathbf{U}^\top = \mathbf{W}\mathbf{A}\mathbf{M}_{\mathcal{S}_k,f_l}(\mathbf{z}(\mathbf{s}))\mathbf{A}^\top\mathbf{W}^\top = \mathbf{V}\mathbf{M}_{\mathcal{S},0}^{-1}(\mathbf{z}(\mathbf{s}))\mathbf{M}_{\mathcal{S}_k,f_l}(\mathbf{z}(\mathbf{s}))\mathbf{V}^\top. \tag{A.7}$$

Therefore, all matrices $\mathbf{V}\mathbf{M}_{\mathcal{S},f_0}^{-1}(\mathbf{z}(\mathbf{s}))\mathbf{M}_{\mathcal{S}_k,f_l}(\mathbf{z}(\mathbf{s}))\mathbf{V}^\top$ for $k = 1,\dots,K$ and $l = 1,\dots,L$ are diagonal.

$\Leftarrow$: For all pairs $i, j = 1,\dots,p$ and $i \neq j$ there exists a pair k, l with $k \in \{1,\dots,K\}$ and $l \in \{1,\dots,L\}$ such that $(\mathbf{M}_{\mathcal{S},f_0}^{-1}(\mathbf{z}(\mathbf{s}))\mathbf{M}_{\mathcal{S}_k,f_l}(\mathbf{z}(\mathbf{s})))_{ii} \neq (\mathbf{M}_{\mathcal{S},f_0}^{-1}(\mathbf{z}(\mathbf{s}))\mathbf{M}_{\mathcal{S}_k,f_l}(\mathbf{z}(\mathbf{s})))_{jj}$. Hence, only choices of $\mathbf{V} = \mathbf{P}\mathbf{S}$ keep all matrices $\mathbf{V}\mathbf{M}_{\mathcal{S},f_0}^{-1}(\mathbf{z}(\mathbf{s}))\mathbf{M}_{\mathcal{S}_k,f_l}(\mathbf{z}(\mathbf{s}))\mathbf{V}^\top$ for $k = 1,\dots,K$ and $l = 1,\dots,L$ diagonal. This is for instance shown in Bachoc et al. (2020). Therefore, $\mathbf{W}\mathbf{A} = \mathbf{P}\mathbf{S}\mathbf{M}_{\mathcal{S},f_0}^{-1/2}(\mathbf{z}(\mathbf{s}))$ which is of the form **PSD**.

$\Rightarrow$: Assume that there exists one pair $i, j \in \{1,\dots,p\}$ with $i \neq j$ where for all pairs k, l with $k = 1,\dots,K$ and $l = 1,\dots,L$, it holds that $(\mathbf{M}_{\mathcal{S},f_0}^{-1}(\mathbf{z}(\mathbf{s}))\mathbf{M}_{\mathcal{S}_k,f_l}(\mathbf{z}(\mathbf{s})))_{ii} = (\mathbf{M}_{\mathcal{S},f_0}^{-1}(\mathbf{z}(\mathbf{s}))\mathbf{M}_{\mathcal{S}_k,f_l}(\mathbf{z}(\mathbf{s})))_{jj}$. W.l.o.g assume that $i = 1$ and $j = 2$ then $\mathbf{V}$ could be a block diagonal matrix with the first block $((1/\sqrt{2}, 1/\sqrt{2},)^\top, (1/\sqrt{2}, -1/\sqrt{2},)^\top)$ and the second block $\mathbf{I}_{p-2}$. This choice of $\mathbf{V}$ still keeps all matrices $\mathbf{V}\mathbf{M}_{\mathcal{S},f_0}^{-1}(\mathbf{z}(\mathbf{s}))\mathbf{M}_{\mathcal{S}_k,f_l}(\mathbf{z}(\mathbf{s}))\mathbf{V}^\top$ for $k = 1,\dots,K$ and $l = 1,\dots,L$ diagonal. But then $\mathbf{V}$ is not of the form **PS** and consequently **WA** is not of the form **PSD**.

Affine equivariance: Consider an affine transformation of $\mathbf{x}(\mathbf{s})$ written as $\mathbf{x}^*(\mathbf{s}) = \mathbf{B}\mathbf{x}(\mathbf{s}) + \mathbf{c}$, where $\mathbf{B}$ is an invertible $p \times p$ matrix. From Ilmonen et al. (2012) Theorem 2.1 it follows that $\mathbf{M}_{\mathcal{S},f_0}^{-1/2}(\mathbf{x}^*(\mathbf{s})) = \mathbf{V}\mathbf{M}_{\mathcal{S},f_0}^{-1/2}(\mathbf{x}(\mathbf{s}))\mathbf{B}^{-1}$, where $\mathbf{V}$ is a unique $p \times p$ orthogonal matrix. The unmixing matrix functional $\mathbf{W}^*(\mathbf{x}^*(\mathbf{s})) = \mathbf{U}^*\mathbf{M}_{\mathcal{S},f_0}^{-1/2}(\mathbf{x}^*(\mathbf{s}))$ maximizes

$$\begin{aligned}&\sum_{k=1}^{K}\sum_{l=1}^{L}\|\mathrm{diag}(\mathbf{U}^*\mathbf{M}_{\mathcal{S}_k,f_l}(\mathbf{x}^{st*}(\mathbf{s}))\mathbf{U}^{*\top})\|_F^2 \\ &= \sum_{k=1}^{K}\sum_{l=1}^{L}\|\mathrm{diag}(\mathbf{U}^*\mathbf{M}_{\mathcal{S},f_0}^{-1/2}(\mathbf{x}^*(\mathbf{s}))\mathbf{M}_{\mathcal{S}_k,f_l}(\mathbf{x}^*(\mathbf{s}))\mathbf{M}_{\mathcal{S},f_0}^{-1/2}(\mathbf{x}^*(\mathbf{s}))\mathbf{U}^{*\top})\|_F^2 \\ &= \sum_{k=1}^{K}\sum_{l=1}^{L}\|\mathrm{diag}(\mathbf{U}^*\mathbf{V}\mathbf{M}_{\mathcal{S},f_0}^{-1/2}(\mathbf{x}(\mathbf{s}))\mathbf{B}^{-1}\mathbf{B}\mathbf{M}_{\mathcal{S}_k,f_l}(\mathbf{x}(\mathbf{s}))\mathbf{B}^\top\mathbf{B}^{-\top}\mathbf{M}_{\mathcal{S},f_0}^{-1/2}(\mathbf{x}(\mathbf{s}))\mathbf{V}^\top\mathbf{U}^{*\top})\|_F^2 \\ &= \sum_{k=1}^{K}\sum_{l=1}^{L}\|\mathrm{diag}(\mathbf{U}^*\mathbf{V}\mathbf{M}_{\mathcal{S}_k,f_l}(\mathbf{x}^{st}(\mathbf{s}))\mathbf{V}^\top\mathbf{U}^{*\top})\|_F^2.\end{aligned} \tag{A.8}$$

Therefore, $\mathbf{U} = \mathbf{U}^*\mathbf{V}$ is the joint diagonalizer of the matrices $\mathbf{M}_{\mathcal{S}_k,f_l}(\mathbf{x}^{st}(\mathbf{s}))$, $k = 1,\dots,K$, $l = 1,\dots,L$. This leads to

$$\begin{aligned}\mathbf{W}^*(\mathbf{x}^*(\mathbf{s})) &= \mathbf{U}^*\mathbf{M}^{-1/2}_{\mathcal{S},f_0}(\mathbf{x}^*(\mathbf{s})) = \mathbf{U}\mathbf{V}^\top\mathbf{V}\mathbf{M}^{-1/2}_{\mathcal{S},f_0}(\mathbf{x}(\mathbf{s}))\mathbf{B}^{-1} = \mathbf{U}\mathbf{M}^{-1/2}_{\mathcal{S},f_0}(\mathbf{x}(\mathbf{s}))\mathbf{B}^{-1}\\ &= \mathbf{W}(\mathbf{x}(\mathbf{s}))\mathbf{B}^{-1},\end{aligned} \tag{A.9}$$

which concludes the proof. □

Appendix B. Simulation results for the skewed setting

Figs. B.9, B.10 and B.11 show the simulation results for the skewed sample location pattern discussed in Sections 4.2, 4.3 and 4.4 respectively. The qualitative results are very similar to the ones of the uniform sample location pattern seen in Figs. 2–4 with two minor differences. Firstly, the overall performance is worsened for all methods due to the imbalanced distribution of the sample locations. Secondly, the SNSS.sd method where the domain is halved across the y axis clearly increases its performance as the sample locations density is still constant along the y axis.

References

Aitchison, J., 2003. The Statistical Analysis of Compositional Data. Blackburn Press.

Anderes, E.B., Stein, M.L., 2011. Local likelihood estimation for nonstationary random fields. J. Multivariate Anal. 102 (3), 506–520. http://dx.doi.org/10.1016/j.jmva.2010.10.010.

Apanasovich, T.V., Genton, M.G., Sun, Y., 2012. A valid Matérn class of cross-covariance functions for multivariate random fields with any number of components. J. Amer. Statist. Assoc. 107 (497), 180–193. http://dx.doi.org/10.1080/01621459.2011.643197.

Bachoc, F., Genton, M.G., Nordhausen, K., Ruiz-Gazen, A., Virta, J., 2020. Spatial blind source separation. Biometrika 107 (3), 627–646. http://dx.doi.org/10.1093/biomet/asz079.

Bailey, T., Krzanowski, W., 2012. An overview of approaches to the analysis and modelling of multivariate geostatistical data. Math. Geosci. 44, 381–393. http://dx.doi.org/10.1007/s11004-011-9360-7.

Cappello, C., De Iaco, S., Palma, M., Pellegrino, D., 2021. Spatio-temporal modeling of an environmental trivariate vector combining air and soil measurements from Ireland. Spatial Stat. 42, 100455. http://dx.doi.org/10.1016/j.spasta.2020.100455.

Cardoso, J., 1989. Source separation using higher order moments. In: International Conference on Acoustics, Speech, and Signal Processing. pp. 2109–2112 vol.4. http://dx.doi.org/10.1109/ICASSP.1989.266878.

Cardoso, J.-F., Souloumiac, A., 1996. Jacobi angles for simultaneous diagonalization. SIAM J. Matrix Anal. Appl. 17 (1), 161–164. http://dx.doi.org/10.1137/S0895479893259546.

Cartone, A., Postiglione, P., 2021. Principal component analysis for geographical data: the role of spatial effects in the definition of composite indicators. Spatial Econ. Anal. 16 (2), 126–147. http://dx.doi.org/10.1080/17421772.2020.1775876.

Choi, S., Cichocki, A., 2000a. Blind separation of nonstationary and temporally correlated sources from noisy mixtures. In: Neural Networks for Signal Processing X. Proceedings of the 2000 IEEE Signal Processing Society Workshop (Cat. No.00TH8501), Vol. 1. pp. 405–414. http://dx.doi.org/10.1109/NNSP.2000.889432.

Choi, S., Cichocki, A., 2000b. Blind separation of nonstationary sources in noisy mixtures. Electron. Lett. 36 (9), 848–849. http://dx.doi.org/10.1049/el:20000623.

Choi, S., Cichocki, A., Belouchrani, A., 2001. Blind separation of second-order nonstationary and temporally colored sources. In: Proceedings of the 11th IEEE Signal Processing Workshop on Statistical Signal Processing (Cat. No.01TH8563). pp. 444–447. http://dx.doi.org/10.1109/SSP.2001.955318.

Comon, P., Jutten, C., 2010. Handbook of Blind Source Separation: Independent Component Analysis and Applications. Academic Press, Amsterdam.

De Iaco, S., Myers, D., Palma, M., Posa, D., 2013. Using simultaneous diagonalization to identify a space–time linear coregionalization model. Math. Geosci. 45, 69–86. http://dx.doi.org/10.1007/s11004-012-9408-3.

Eriksson, J., Koivunen, V., 2004. Identifiability, separability, and uniqueness of linear ICA models. IEEE Signal Process. Lett. 11 (7), 601–604. http://dx.doi.org/10.1109/LSP.2004.830118.

Filzmoser, P., Hron, K., Templ, M., 2018. Applied Compositional Data Analysis. with Worked Examples in R. Springer.

Gelfand, A.E., Schmidt, A.M., Banerjee, S., Sirmans, C.F., 2004. Nonstationary multivariate process modeling through spatially varying coregionalization. Test 13, 263–312. http://dx.doi.org/10.1007/BF02595775.

Genton, M.G., Kleiber, W., 2015. Cross-covariance functions for multivariate geostatistics. Statist. Sci. 30 (2), 147–163. http://dx.doi.org/10.1214/14-STS487.

Gneiting, T., Kleiber, W., Schlather, M., 2010. Matern cross-covariance functions for multivariate random fields. J. Amer. Statist. Assoc. 105, 1167–1177. http://dx.doi.org/10.1198/jasa.2010.tm09420.

Goovaerts, P., 1992. Factorial kriging analysis: A useful tool for exploring the structure of multivariate spatial soil information. J. Soil Sci. 43 (4), 597–619. http://dx.doi.org/10.1111/j.1365-2389.1992.tb00163.x.
Goulard, M., Voltz, M., 1992. Linear coregionalization model: Tools for estimation and choice of cross-variogram matrix. Math. Geol. 24, 269–286. http://dx.doi.org/10.1007/BF00893750.
Guttorp, P., Gneiting, T., 2006. Studies in the history of probability and statistics XLIX on the Matérn correlation family. Biometrika 93 (4), 989–995. http://dx.doi.org/10.1093/biomet/93.4.989.
Harris, P., Clarke, A., Juggins, S., Brunsdon, C., Charlton, M., 2015. Enhancements to a geographically weighted principal component analysis in the context of an application to an environmental data set. Geogr. Anal. 47 (2), 146–172. http://dx.doi.org/10.1111/gean.12048.
Illner, K., Miettinen, J., Fuchs, C., Taskinen, S., Nordhausen, K., Oja, H., Theis, F.J., 2015. Model selection using limiting distributions of second-order blind source separation algorithms. Signal Process. 113, 95–103. http://dx.doi.org/10.1016/j.sigpro.2015.01.017.
Ilmonen, P., Nordhausen, K., Oja, H., Ollila, E., 2010. A new performance index for ICA: Properties, computation and asymptotic analysis. In: Vigneron, V., Zarzoso, V., Moreau, E., Gribonval, R., Vincent, E. (Eds.), Latent Variable Analysis and Signal Separation. Springer, pp. 229–236. http://dx.doi.org/10.1007/978-3-642-15995-4_29.
Ilmonen, P., Oja, H., Serfling, R., 2012. On invariant coordinate system (ICS) functionals. Internat. Statist. Rev. 80 (1), 93–110. http://dx.doi.org/10.1111/j.1751-5823.2011.00163.x.
Jiang, Z., 2019. A survey on spatial prediction methods. IEEE Trans. Knowl. Data Eng. 31 (9), 1645–1664. http://dx.doi.org/10.1109/TKDE.2018.2866809.
Kleiber, W., Nychka, D., 2012. Nonstationary modeling for multivariate spatial processes. J. Multivariate Anal. 112, 76–91. http://dx.doi.org/10.1016/j.jmva.2012.05.011.
Li, J., Heap, A.D., 2014. Spatial interpolation methods applied in the environmental sciences: A review. Environ. Model. Softw. 53, 173–189. http://dx.doi.org/10.1016/j.envsoft.2013.12.008.
Lietzen, N., Virta, J., Nordhausen, K., Ilmonen, P., 2020. Minimum distance index for BSS, generalization, interpretation and asymptotics. Austrian Journal of Statistics 49 (4), 57–68. http://dx.doi.org/10.17713/ajs.v49i4.1130.
Miettinen, J., Nordhausen, K., Taskinen, S., 2017. Blind source separation based on joint diagonalization in R: The packages JADE and bssasymp. J. Stat. Softw. 76 (2), 1–31. http://dx.doi.org/10.18637/jss.v076.i02.
Miettinen, J., Taskinen, S., Nordhausen, K., Oja, H., 2015. Fourth moments and independent component analysis. Statist. Sci. 30 (3), 372–390. http://dx.doi.org/10.1214/15-STS520.
Muehlmann, C., Bachoc, F., Nordhausen, K., Yi, M., 2020. Test of the latent dimension of a spatial blind source separation model. arXiv:2011.01711.
Muehlmann, C., Fačevicová, K., Gardlo, A., Janečková, H., Nordhausen, K., 2021a. Independent component analysis for compositional data. In: Daouia, A., Ruiz-Gazen, A. (Eds.), Advances in Contemporary Statistics and Econometrics: Festschrift in Honor of Christine Thomas-Agnan. Springer, Cham, pp. 525–545. http://dx.doi.org/10.1007/978-3-030-73249-3_27.
Muehlmann, C., Filzmoser, P., Nordhausen, K., 2021b. Spatial blind source separation in the presence of a drift. arXiv:2108.13813.
Muehlmann, C., Nordhausen, K., Virta, J., 2021c. SpatialBSS: Blind source separation for multivariate spatial data. R package version 0.12-0, URL https://CRAN.R-project.org/package=SpatialBSS.
Muehlmann, C., Nordhausen, K., Yi, M., 2021d. On cokriging, neural networks, and spatial blind source separation for multivariate spatial prediction. IEEE Geosci. Remote Sens. Lett. 18 (11), 1931–1935. http://dx.doi.org/10.1109/LGRS.2020.3011549.
Nordhausen, K., 2014. On robustifying some second order blind source separation methods for nonstationary time series. Statist. Papers 55 (1), 141–156. http://dx.doi.org/10.1007/s00362-012-0487-5.
Nordhausen, K., Oja, H., 2018. Independent component analysis: A statistical perspective. WIREs: Comput. Stat. 10, e1440. http://dx.doi.org/10.1002/wics.1440.
Nordhausen, K., Oja, H., Filzmoser, P., Reimann, C., 2015. Blind source separation for spatial compositional data. Math. Geosci. 47 (7), 753–770. http://dx.doi.org/10.1007/s11004-014-9559-5.
Nordhausen, K., Virta, J., 2019. An overview of properties and extensions of FOBI. Knowl.-Based Syst. 173, 113–116. http://dx.doi.org/10.1016/j.knosys.2019.02.026.
Pan, Y., Matilainen, M., Taskinen, S., Nordhausen, K., 2021. A review of second-order blind identification methods. WIREs Comput. Stat. n/a, e1550. http://dx.doi.org/10.1002/wics.1550.
Pfister, N., Weichwald, S., Bühlmann, P., Schölkopf, B., 2019. Robustifying independent component analysis by adjusting for group-wise stationary noise. J. Mach. Learn. Res. 20 (147), 1–50. http://dx.doi.org/10.3929/ethz-b-000374036.
Reimann, C., Birke, M., Demetriades, A., Filzmoser, P., O'Connor, P. (Eds.), 2014. Chemistry of Europe's agricultural soils, Part A. Schweizerbart Science Publishers.
Sampson, P.D., 2010. Constructions for nonstationary spatial processes. In: Gelfand, A.E., Diggle, P.J., Fuentes, M., Guttorp, P. (Eds.), Handbook of Spatial Statistics. CRC Press, Boca Raton, pp. 119–130. http://dx.doi.org/10.1201/9781420072884-c9.
Schlather, M., Malinowski, A., Menck, P.J., Oesting, M., Strokorb, K., 2015. Analysis, simulation and prediction of multivariate random fields with package RandomFields. J. Stat. Softw. 63 (8), 1–25. http://dx.doi.org/10.18637/jss.v063.i08.
Team, R.C., 2019. R: A Language and Environment for Statistical Computing. R Foundation for Statistical Computing, Vienna, Austria, URL https://www.R-project.org/.
Thakur, M., Samanta, B., Chakravarty, D., 2018. A non-stationary geostatistical approach to multigaussian kriging for local reserve estimation. Stoch. Environ. Res. Risk Assess. 32, 2381–2404. http://dx.doi.org/10.1007/s00477-018-1533-1.
Tong, L., Liu, R., Soon, V.C., Huang, Y., 1991. Indeterminacy and identifiability of blind identification. IEEE Trans. Circuits Syst. 38 (5), 499–509. http://dx.doi.org/10.1109/31.76486.

Vu, Q., Zammit-Mangion, A., Cressie, N., 2021. Modeling nonstationary and asymmetric multivariate spatial covariances via deformations. ArXiv 2004.08724.

Wackernagel, H., 2003. Multivariate Geostatistics. Springer.

Wang, H., Guan, Y., Reich, B., 2019. Nearest-neighbor neural networks for geostatistics. In: Proceedings of the 2019 International Conference on Data Mining Workshops. ICDMW, pp. 196–205. http://dx.doi.org/10.1109/ICDMW.2019.00038.